Metadata of the Book that will be visualized online

Book Title	Dynamics of Soft Matter	
Book SubTitle	Neutron Applications	
Copyright Year	2012	
Copyright Holder	Springer Science+Business Media, LLC	
Corresponding Author	Family Name	**Longeville**
	Particle	
	Given Name	**Stéphane**
	Suffix	
	Division	Laboratoire Léon Brillouin
	Organization	CEA Saclay
	Address	F-91191 Gif sur Yvette, Cedex, France
	Email	
Author	Family Name	**Doster**
	Particle	
	Given Name	**Wolfgang**
	Suffix	
	Division	Technische Universität München
	Organization	Physik Department E 13
	Address	James Franck Strasse 1, D-85747, Garching, Germany
	Email	

Author's Proof

Chapter 8
Protein Dynamics and Function

Stéphane Longeville and Wolfgang Doster

UNCORRECTED PROOF

8.1 Introduction

Proteins were discovered by the Dutch chemist G. Mulder as early as 1838. They were named by J. J. Berzelius from the Greek word *Protos*, which signifies first in importance, probably because they constitute more than 50% of the dry weight of the cells. Another explanation suggests that proteins (like protean) arise form the Greek god *Proteus* who has the capability to appear under different forms. This refers to the very strong variety of protein structures but such an approach is an anachronism because protein structures were only studied during the twentieth century.

Proteins are ubiquitous in cells and serve all types of metabolism and function: they can be structural proteins, help transport or catalyse reactions and also be involved in regulation and signal pathways or act as molecular motors. Proteins are biological macromolecules composed of one or several chains of amino acids whose amino acid sequences are coded by the genome and constitute the primary structure of the proteins. To achieve their function, most of them must reach a unique structure by a folding mechanism, which is not fully understood and is a very active field of structural biology.

AQ1

S. Longeville (✉)
Laboratoire Léon Brillouin, CEA Saclay, F-91191 Gif sur Yvette Cedex, France
e-mail: slongeville@cea.fr

W. Doster
Technische Universität München, Physik Department E 13, James Franck Strasse 1, D-85747 Garching, Germany
e-mail: wdoster@ph.tum.de

V.G. Sakai et al. (eds.), *Dynamics of Soft Matter: Neutron Applications*, Neutron Scattering Applications and Techniques, DOI 10.1007/978-1-4614-0727-0_8,
© Springer Science+Business Media, LLC 2012

Author's Proof

The structure–function relationship alone does not account for protein activity, since structural fluctuations and conformational adjustments are required to adapt to the conversion of substrate molecules and regulation. Biological physics is based on soft interactions dominated by $k_B T$ at ambient temperature. Thus "cold" neutrons with typical wavelengths of 5–10 $\AA$, and energies of a few meV allow the study of atomic and molecular structures together with their motions. In contrast, the typical energies of photons at atomic wavelengths, X-rays, are in the range of keV far above $k_B T$. It is also interesting to notice that low-temperature measurements on biological objects will be necessary to unravel the different dynamical mechanisms by time separation or study of the activation energies. Therefore, high energy resolution of some neutron spectrometers will be relevant for biological physics. Small angle neutron scattering has now been used for more than 40 years [1] to unravel the structure of proteins in solution or in crystal form. Inelastic and quasielastic neutron scattering investigations of proteins really started with the study of dynamical transition in hydrated powders [2] and has developed over the past 20 years to measurements of protein diffusion in vivo [3].

The information on the structure and dynamics of macromolecules obtained from a neutron experiment are fully described by the dynamical structure factor $S(\mathbf{Q}, \omega)$ in the frequency domain, or equivalently the intermediate scattering function, I($\mathbf{Q}$,t), in the time domain. These have been described in the previous chapters. These two functions are generally very difficult to manage since they are composed of contributions from the different dynamical processes weighted by the atomic scattering length. A given scattering centre inside a protein performs different types of motions including Brownian translational and rotational motions, large-scale internal and small group fluctuations and high-frequency oscillations. This leads to a complicated dynamical function (or intermediate scattering function depending on the type of measurement). To separate the different types of motion it is necessary to use different types of samples (powder, solutions, in-cell measurements, etc.) as well as employ various spectrometers with different wave vector and frequency ranges. In addition, the large difference in scattering length densities between hydrogen and deuterium, can be used to either hide the contribution of some molecules (for example, the water) or selectively probe self- or collective dynamics, for example. The signal is separated into incoherent scattering functions which measure the self-correlation of all atoms in the sample and coherent ones, probing the pair-correlation function of all centres.

AQ2

For a solution of biomacromolecules such as proteins, the motions are generally separated into global and internal motions. The former include generally translational and rotational Brownian diffusion, which depends at very low concentration on the temperature, a friction term as a function of the solvent viscosity and the shape of the macromolecule. The latter includes all low-frequency and high-frequency modes of motions together with possible large amplitude domain motions overdamped due to the friction with the solvent.

UNCORRECTED PROOF

Author's Proof

8.2 Protein-Internal Motions

Most proteins contain an active site, which is generally shielded from the solvent, thus providing a unique environment for chemical reactions. However, the substrate and product molecules must enter and leave the protein site, which involves the solvent. The main goal of this chapter is to demonstrate that protein-internal motions and functional processes can be classified into two types:

Class 1 are those solvent-decoupled processes which represent truly internal motions. In contrast, the rates of class 2 motions vary with the viscosity of the solvent near the protein surface.

8.2.1 Protein-Internal Structural Motions and Biological Function

We start the chapter on protein-internal motions with a detailed look at protein function. Each protein has its unique function, so there is no general definition, that applies to all proteins. The notion of "biological function" denotes an overall process, which is composed of several elementary steps. For instance, the loss of proteolytic activity of the protein "lysozyme" below a critical degree of hydration (0.25 g water/g protein), less than a monolayer, is often attributed the loss of water-mediated motion at the active site [4]. A more likely reason for the loss in apparent activity is the transfer of substrate molecules, which is arrested at low hydration. In the following, we define protein function as a protein-assisted multi-step process involving a small ligand molecule: Several elementary steps contribute to the overall reaction, which defines the protein activity:

- The ligand in solution is transfered across the protein-solvent interface
- The ligand migrates through the protein structure to the active site and
- The ligand binds to the active site, where it is chemically transformed

To complete the functional cycle, also the reverse reactions must happen: the dissociation of the possibly modified ligand from the active site, migration through the protein matrix and release to the solvent. Since proteins are close-packed structures, the incorporation of a ligand may induce a structural reorganization assisted by small-scale fluctuations. Here, packing defects in the otherwise dense protein structure play an important role.

This issue has been extensively studied with the heme protein, myoglobin. It reversibly binds gas ligands at the heme site, which is buried from the solvent in the protein matrix. The heme–iron binding site, blue in Fig. 8.1, is thus not directly accessible to the ligands.The "arms" of the heme group, however, the polar propionic acid side chains, reach out into the solvent and couple the heme displacements to motions in the solvent [5].

UNCORRECTED PROOF

Author's Proof

AQ3

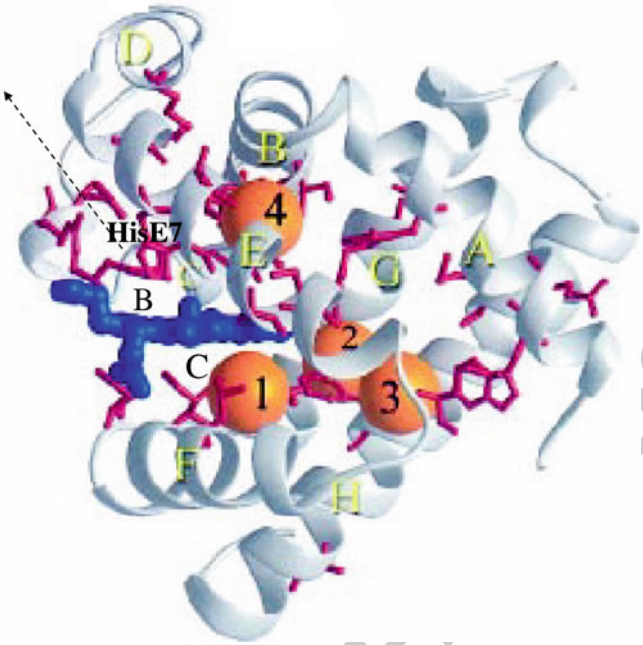

this figure will be printed in b/w

Fig. 8.1 Secondary structure of the oxygen storage protein myoglobin with helices A–F, the heme group (blue), which binds oxygen, the xenon-binding cavities 1–4 (orange), the distal His64 (E7), the distal cavity docking site B and the proximal docking site C. The arrow denotes the most probable ligand escape pathway into the solvent. via the distal gate of His64

UNCORRECTED PROOF

Because gas ligands must find their way to the heme by migrating through dense protein structure, structural fluctuations and internal cavities are required to facilitate ligand binding. With X-ray scattering various cavities in myoglobin were discovered, which act as xenon binding sites. These Xe-docking sites turned out to be crucial to the tranfer of small gas ligands like dioxygen of CO inside the protein [6, 7]. The four major Xe-binding sites are indicated in Fig. 8.1. Time-resolved X-ray crystallography of the photolysed Mb–CO complex and molecular dynamics simulations have established a series of ligand dockings sites and their time sequence [8–12]:

After photolysis from the Fe-binding site A, the CO-molecule occupies the distal pocket B (Fig. 8.1) from which it can rebind to A, or escape to the solvent S via the distal gate of HisE7. Rebinding from the solvent S $\rightarrow$A is the slowest process. An alternative route from B involves the transfer via cavity Xe4 to the proximal site of the heme, Xe1 or Xe2. In the latter case, rebinding occurs from the kinetic state C $\rightarrow$A. Further exit pathways involving Xe3 have been identified by simulations [10–12]. The kinetic results can be represented by Gibsons four state model [7]:

$$\begin{array}{ccc} \mathbf{S} & \rightleftharpoons & \mathbf{B} \rightleftharpoons \mathbf{C} \\ & & \updownarrow \\ & & \mathbf{A} \end{array}$$

Author's Proof

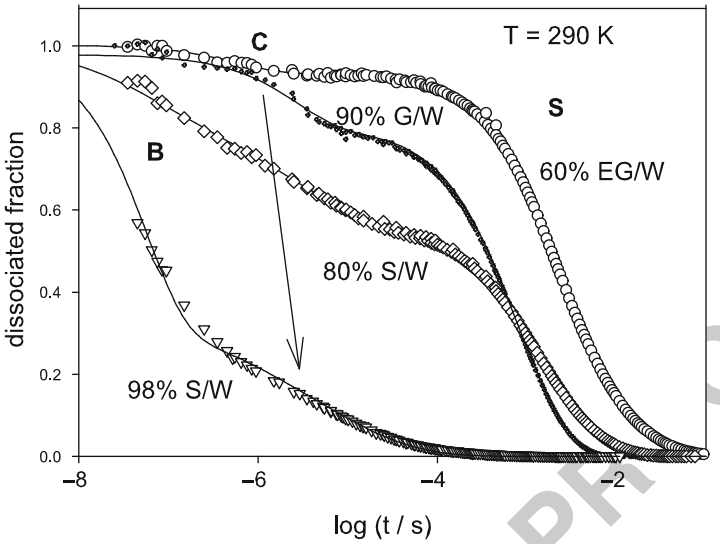

Fig. 8.2 The recombination kinetics of carbon monoxide (CO) to the heme iron of myoglobin after dissociation by a laser flash in various solvents with different viscosity: 60% (by weight) ethylenglycol/water, 90% glycerol–water, 80% sucrose–water and 98% sucrose–water. Three kinetic intermediates according to the scheme are indicated: S (solvent), B (distal pocket), C (protein matrix and proximal site). The arrow emphasizes the constant time position of the C-intermediate with increasing solvent viscosity

In the following, we discuss the action of the solvent, and of the solvent viscosity in particular, on elementary steps of CO-binding to myoglobin. For this purpose, we have reevaluated the early flash-photolysis experiments of Kleinert et al. according to Gibsons kinetic scheme [4, 13, 14].

Figure 8.2 displays the recombination kinetics of CO + myoglobin after a nanosecond laser flash in solvents of varying viscosity. The three kinetic intermediates, B, C and S, are also indicated. The arrow points towards a drastic increase in the solvent viscosity. The main effect of viscosity on the kinetics is the reduction in the amplitude of the slowest process, the external rebinding from the solvent, S→A.

The amplitude of S→A is equal to the escape fraction of ligands, $N_{out} \leq 1$, which leave the protein after photolysis instead of rebinding internally. A decrease of N_{out} indicates, that the ligand exit rate across the protein–solvent interface decreases with the external viscosity. At 90% sucrose-water, the solvent is in a glassy state at 290 K. Below the glass temperature $T_g \approx 325$ K, the viscosity is infinite, thus $N_{out} \approx 0$. As Fig. 8.2 shows, that the internal (geminate) recombination process and ligand migration involving the decay of the intermediates B and C are still operating in spite of a glassy external environment. The rate of C → A seems to be rather independent of the solvent viscosity. The amplitude of the fast geminate recombination from the heme pocket B → A, increases with the solvent viscosity in compensation to a decreasing N_{out}. Figure 8.3 shows several internal transition rates versus the external

UNCORRECTED PROOF

Author's Proof

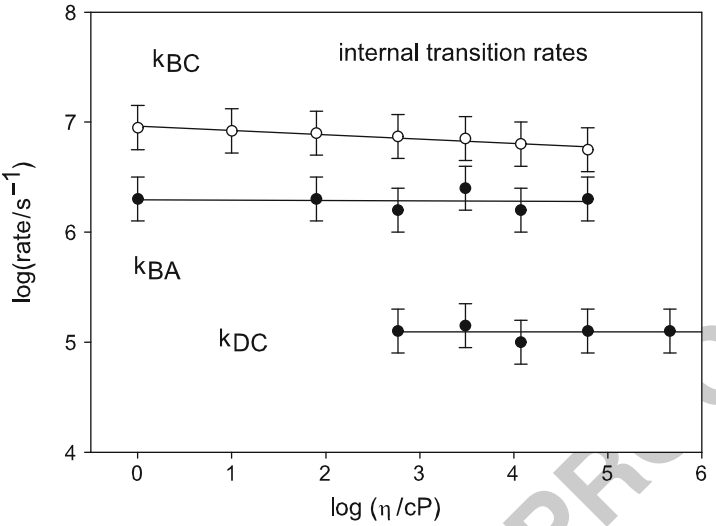

Fig. 8.3 Internal transition rates of CO in myoglobin at 290 K versus the external solvent viscosity according to the four state model

viscosity, evaluated according to the kinetic four-state model: The formation of the covalent bond at the heme iron (B→A) and the crossing rate from the distal to proximal site of the heme k_{BC} are independent of the viscosity. Since the intercavity migration of the CO molecule requires structural adjustments, one has to invoke the existence of class 1 structural fluctuations, which are decoupled from the solvent. On the other hand, the exit and entry rates belong to class 2 fluctuations, which are strongly coupled to the solvent [14]. The viscosity of various biosolvents versus the temperature is given in Fig. 8.4 [13].

The data were obtained from a combination of viscosity and specific heat spectroscopy experiments. The relaxation rate and viscosity are related by the Maxwell equation [13, 14]:

$$\eta = g_\infty \cdot T \cdot \tau_s, \tag{8.1}$$

where g_∞ denotes the high frequency bulk modulus, $\approx 10^9 \left[\mathrm{cP \cdot K^{-1} s^{-1}}\right]$ [13].

Figure 8.5 displays CO-exit rates from horse myoglobin versus the viscosity in several solvents. The viscosity in a given solvent is modified by varying the temperature. In addition to a dependence of viscosity, the exit rates also depend on a protein intrinsic barrier of $H_{BS} \approx 25$ kJ/mol [13, 14]. For this reason, the absolute values of k_s and k_{BS} differ by a factor of 100. To compare the exit rates between different solvents, the data were corrected to a common temperature of 290 K based on Kramer's law of activated escape [14]:

$$k_{BS} = \frac{A}{\eta_s} \cdot \exp\left(-H_{BS}/RT\right) \tag{8.2}$$

UNCORRECTED PROOF

Author's Proof

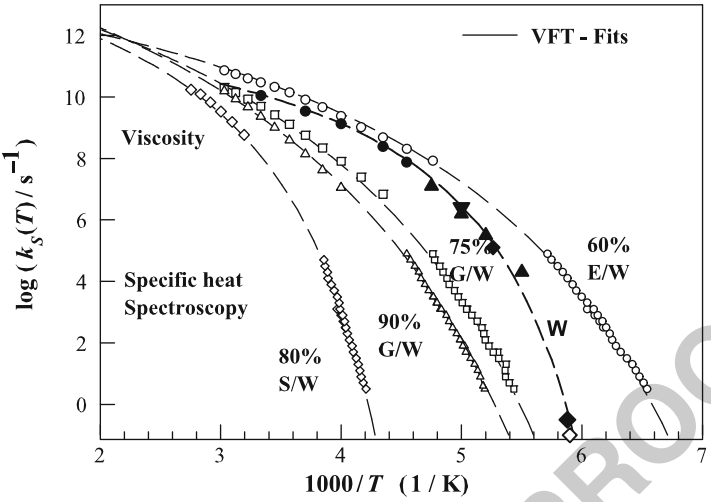

Fig. 8.4 Solvent relaxation rates $k_s \propto 1/\eta$ derived from viscosity and specific heat spectroscopy experiments ref.[13]. Acronyms: S(sucrose), W(water), G(glycerol), E(ethylene glycol). Myoglobin hydration water was measured with neutron scattering [14]. Lines are fits to a super-Arrhenius VFT law, (8.11)

A is a prefactor and η_s denotes the viscosity near the protein surface. The results are also shown in Fig. 8.5. In glycerol-water, the CO-exit (and entry) rates vary with the inverse of the bulk viscosity $k_{BS} \propto 1/\eta$. Moreover, the respective values of $k_{BS}(\eta)$ fall right on top of each other, at least at high viscosity. This shows that the bulk viscosity is the essential parameter, while the chemical composition plays a minor role. These processes thus belong to class 2. In contrast, in the 80% sucrose-water solution, the exit rates vary less than the reciprocal bulk viscosity and may exceed k_s at high viscosity. Such reduced viscosity effects have been interpreted as indicating a fractional solvent exposure of the reaction, leading a sublinear power law [16]. However, the cosolvent sucrose is known to be partially excluded from the protein domain. The thermodynamic experiments of Timasheff and collaborators have shown that the concentration of cosolvents near the protein surface can be different from the bulk [17]. Some cosolvents like sucrose are more excluded than others from the protein domain, leading to a reduced viscosity near the surface as compared to the bulk [5, 13, 14, 17]. This exclusion can explain the observed sublinear viscosity effect and the dependence like: $\eta_s = \eta_{bulk}^{\kappa}$ with the exponent $\kappa \leq 1$. At lower viscosities the CO-exit rates in glycerol-water and in dilute aqueous solution deviate however from a $1/\eta$ law. In this regime, the escape of CO, which requires the displacement of solvent molecules to create a cavity, becomes less and less rate-limiting. Ansari et al. report on a similar viscosity dependence of a conformational transition rate of myoglobin, which nearly coincides with the CO-exit rate as shown in Fig. 8.4 [15]. The onset of a plateau, which they observe at low viscosity, has been attributed to the influence of an protein-internal viscosity.

UNCORRECTED PROOF

Author's Proof

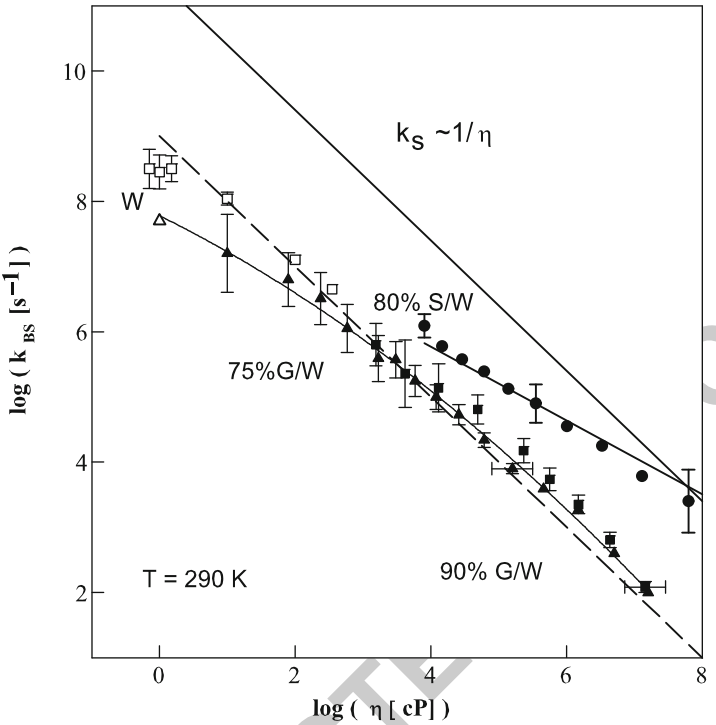

Fig. 8.5 CO-exit rates k_{BS} versus viscosity in several solvents, reevaluated experiments of ref. [13] corrected to 290 K: open triangle: in aqueous solution, filled triangle: 75% glycerol-water, full squares: 90% glycerol-water, full circles: 80% sucrose-water, open squares: rate of conformational change of myoglobin in 56 and 79% glycerol-water [15], full line: solvent relaxation rate k_s in 75% glycerol-water [14]

We thus arrive at the simple and basic conclusion, that the kinetics of ligand binding to myogobin can be decomposed into elementary steps, which belong either to class 1 (internal) or to class 2.

It was anticipated, that the CO migration requires the assistance of structural fluctuations. We thus turn to the question, whether a similar classification into two classes can be performed with structural relaxation processes in myoglobin. An important class of fluctuations refers to displacements of the heme group, which is the active site. With Mössbauer spectroscopy, one can derive displacement fluctuations of the heme iron on a nanosecond time scale [5,18,19]. Results obtained with different solvents are shown in Fig. 8.6a: The displacements follow a linear temperature dependence reflecting vibrational motions independent of the protein environment. Above about 200 K a dynamical transition occurs, the displacements increase, because structural relaxation processes are being increasingly resolved within the pico- to nanosecond window of the spectrometer. Most interesting, the onset of the transition depends on the solvent composition: While myoglobin

UNCORRECTED PROOF

Author's Proof

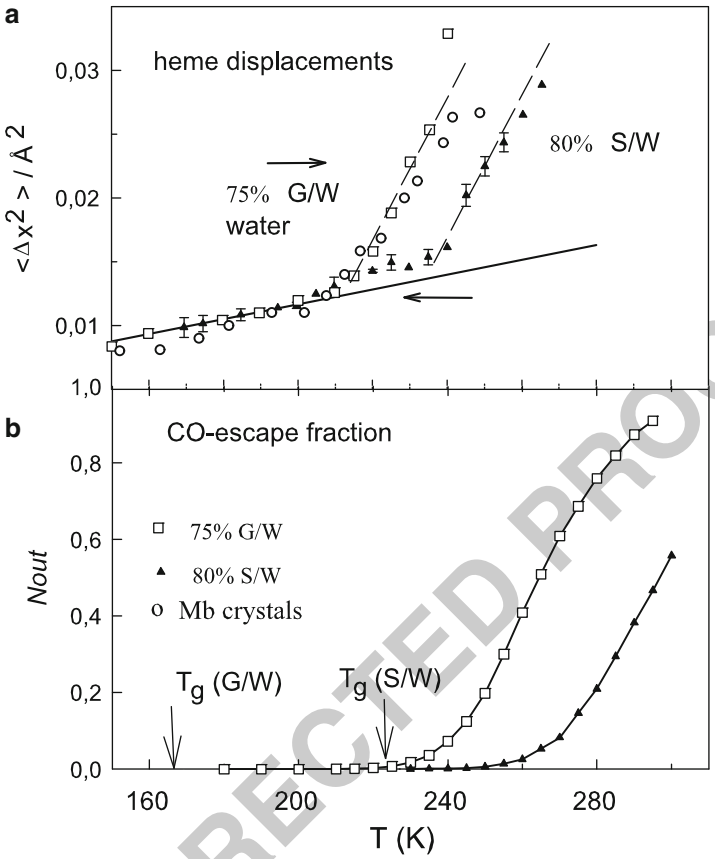

Fig. 8.6 (**a**) Dynamcial transition and mean square displacements of the heme of myoglobin from Mössbauer spectroscopy in myoglobin crystals (open circles), 75% glycerol-water (open squares) and 80% sucrose-water (triangles) [5] (**b**) Solvent escape fraction N_{out} of CO after photolysis from myoglobin in 75 and 90% glycerol-water [14]

UNCORRECTED PROOF

crystals and myoglobin in a 75% glycerol-water solution exhibit a common onset temperature of $T_\Delta \approx 210$ K, with the more viscous solvent 80% sucrose-water one observes that the onset is shifted to a higher temperature of $T_\Delta = 240$ K. The motion of the heme group thus belongs to class 2 fluctuations. One type of heme-solvent coupling could occur directly via its polar side chains or indirectly via protein-matrix fluctuations.

Figure 8.6 also displays the respective bulk glass temperatures. The structural relaxation time at T_g is in the range seconds and the viscosity approaches 10^{13} Poise. The same α-process is presumably probed by Mössbauer spectroscopy on a much faster time scale, the respective time resolution is the nuclear life time of the ^{57}Fe nucleus of 140 ns. This time shift leads to an upshift in the onset temperature of recorded relaxational displacements from T_g to T_Δ. One should expect that the

Author's Proof

bulk solvent viscosities at the onset temperatures are equivalent. The sucrose-water system however has a much higher bulk viscosity at 240 K than glycerol-water at 210 K. This discrepancy suggests as above, that the surface viscosity is drastically lower with protein-sucrose-water than the bulk value due to preferential hydration [5]. Fig. 8.6b) relates the structural coordinate of heme displacements to a functional parameter, the ligand escape fraction N_{out}. The kinetic onset shows a similar upshift in T_Δ in the more viscous solvent. N_{out} is also a dynamic quantity, reflecting the partitioning between ligand escape and internal rebinding. In the four state model, it can be approximated by:

$$N_{\text{out}} = k_{\text{BS}}(\eta)/(k_{\text{BA}} + k_{\text{BC}} + k_{\text{BS}}(\eta)). \tag{8.3}$$

At the onset temperature of 250 K with 75% glycerol-water, k_{BA} is approximately 2×10^6 s^{-1} and k_{BS} amounts to 2×10^5 s^{-1}, while k_{BC} can be neglected, yielding for $N_{out} \approx 0.1$. This is close to the observed value of N_{out} at 250 K. In this case, the relevant biological "resolution" time is set by the solvent-independent internal binding rate k_{BA}. Biological function turns on, when the escape rate starts to exceed the internal binding rate. On this biologically relevant time scale, the "dynamic transition" occurs at 250 K with 75% glycerol-water solvent. In the next section, we investigate other structural processes of myoglobin probed by elastic and quasi-elastic neutron scattering.

8.2.2 *Dynamical Structural Distributions in Proteins*

In the following we show how the displacement distribution can be reconstructed from experimental neutron scattering functions based on a moment expansion [4, 20, 21]. We again use myoglobin in various environments. As with kinetic experiments, one can discriminate between class 1 and class 2 type fluctuation according to their coupling to the solvent. The neutron scattering cross-section of D_2O-hydrated proteins is dominated (95%) by the non-exchangeable hydrogen atoms and thus incoherent scattering. The corresponding self-intermediate scattering function, $I_s(\mathbf{Q},t)$ records displacements of individual hydrogen atoms (j) [4, 21]:

$$I_s(\mathbf{Q},t) = \langle \exp(i\mathbf{Q}\mathbf{r}_j(0)) \cdot \exp(-i\mathbf{Q}\mathbf{r}_j(t)) \rangle \tag{8.4}$$

The scattering vector $\mathbf{Q}$ is the instrumental parameter to modify the spatial scale probed by the scattering process.

From $I_s(\mathbf{Q},t)$ one derives by a Fourier transform the displacement distribution function $G_s(\mathbf{r},t)$:

$$G_s(\mathbf{r},t) = \int \frac{d^3Q}{(2\pi)^3} \exp(-i\mathbf{Q}\mathbf{r}) \cdot I_s(\mathbf{Q},t) \tag{8.5}$$

UNCORRECTED PROOF

Author's Proof

It denotes the probability density, that atom (j), which is initially at $\mathbf{r}_0$ moves to a position $\mathbf{r}$ within a time interval t, averaged over all atoms j: For a classical system, this is equivalent to:

$$G_s(\mathbf{r},t) = \int d^3 r_0 \, p(\mathbf{r}_0 + \mathbf{r}, \mathbf{r}_0, t) \cdot p_0(\mathbf{r}_0) \tag{8.6}$$

with the equilibrium distribution

$$p_0(\mathbf{r}) = p(\mathbf{r}, \mathbf{r}_0, t = \infty) \tag{8.7}$$

The displacement distribution is defined as the long time value of equ. 9:

$$G_s(\mathbf{r}, t \to \infty) = \int \frac{d^3 Q}{(2\pi)^3} \exp(-i\mathbf{Q}\mathbf{r}) \cdot I_s(\mathbf{Q}, t \to \infty) \tag{8.8}$$

The long-time value of the intermediate scattering function is the so-called elastic incoherent structure factor EISF(Q). The displacement distribution is thus the Fourier transform of the EISF(Q), which represents the fraction of the elastic scattering component in the frequency domain at infinite instrumental resolution. Due to limitations of the experimental Q (and time)-range, a direct transform according to (8.11) is rarely possible. Approximations such as a model-independent moment expansion of the $G(r,t)$ can be useful [4] or specific dynamical models, which account for the molecular structure. The experimental elastic fraction is generally convoluted with the resolution function and is thus not identical with the EISF(Q). In the following, we discuss models of the following intermediate scattering function,

$$I(Q,t) = EISF(Q) + \{1 - EISF(Q)\} \cdot \Phi(t), \tag{8.9}$$

which separates the time- and Q-dependence of the spectrum, since for local molecular processes the time correlation function Φ(t) is independent of Q. Also $\Phi(t \to \infty) = 0$. The EISF(Q) contains information on the geometry of the motion, which is a fingerprint of a molecular process.

We focus on experiments performed with myoglobin, embedded in three different environments: (a) water: fully hydrated (0.35 g D_2O / g protein) (b) vacuum (lyophilized to less than 0.05 g/g) and (c) a glassy perdeuterated glucose matrix, $T_g = 325$ K. The backscattering spectrometer IN13 (ILL, Grenoble) provides an unusually large Q-range of up to 5 $\AA^{-1}$. Figure 8.7 shows representative scattering data approximating the intermediate scattering function I(Q, t = 50 ps) at fixed time at various temperatures in the three environments.

Dehydrated and glassy myoglobin display similar scattering functions, while hydration leads to an additional decrease in the scattering function at high Q.

UNCORRECTED PROOF

Author's Proof

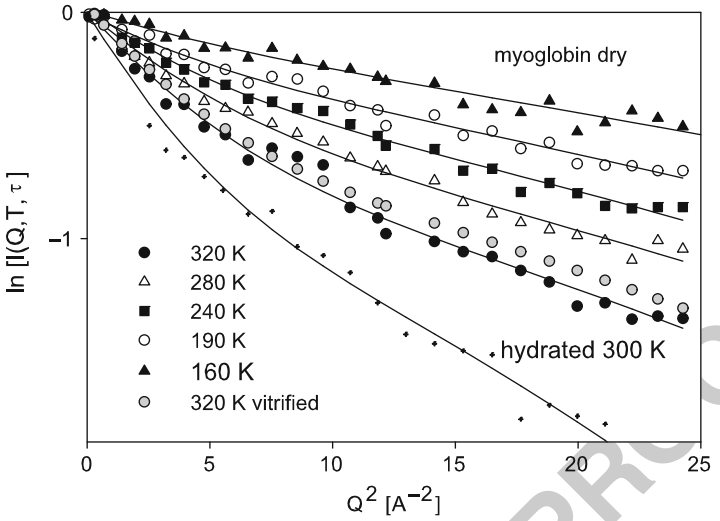

Fig. 8.7 Experimental I(Q, $\tau = 50$ ps) of myoglobin in three different environments, vacuum (dehydrated), vitrified (perdeuterated glucose glass) and D_2O-hydrated (0.35 g/g) using the thermal backscattering spectrometer IN13 at the ILL in Grenoble and fits to a three-fold rotation (methyl group). The data are corrected for multiple scattering

The data could be well represented by a combination of Gaussian displacements, $\langle \Delta x^2_{\text{trans}} \rangle$ and three-fold rotatational jumps according to:

$$EISF(Q) = \exp\left\{-Q\left\langle \Delta x^2_{\text{trans}}\right\rangle\right\} \cdot \left[1 - a + \frac{a}{3}\left(1 + 2 \cdot \frac{\sin\left(\sqrt{3}Q \cdot r\right)}{\sqrt{3}Q \cdot r}\right)\right] \qquad (8.10)$$

This choice is motivated by the fact that methyl groups in proteins carry almost 30% of the total neutron cross-section. This fact is accounted for by the factor a $\approx$0.27 in 8.13. Figure 8.8a shows the elastic fraction of Fig. 8.7 (hydrated myoglobin) now separating the two components, gaussian and rotational, according to 8.13. In particular the rotational component approximates the EISF(Q) of a three-fold rotation quite well, which is assigned to methyl group torsional transitions. Here the wide Q-range of the back-scattering spectrometer IN13 (at the ILL, France) is quite essential. Also shown in Fig. 8.8 are data from the backscattering spectrometer HFBS at the NCNR, NIST (USA). With such a limited Q-range, no assignments are possible. The interpretation of these data by Roh et al. [22] are thus at best an educated guess. The transition rates are shown in the Arrhenius plot of Fig. 8.8b. Both quantities, the EISF and the torsional rates, are required to establish a meaningful intermediate scattering function. The full lines in Fig. 8.7 represent such fits at fixed resolution time, τ_Δ, based on the data in Fig. 8.8.

To transform the apparent EISF(Q) to the spatial domain (8.8), we approximate the data in Fig. 8.7 by a sum of Gaussian functions. Figure 8.9 displays the resulting displacement distribution functions at various temperatures referring to a fixed instrumental time window of $\approx$50–100 ps.

UNCORRECTED PROOF

Author's Proof

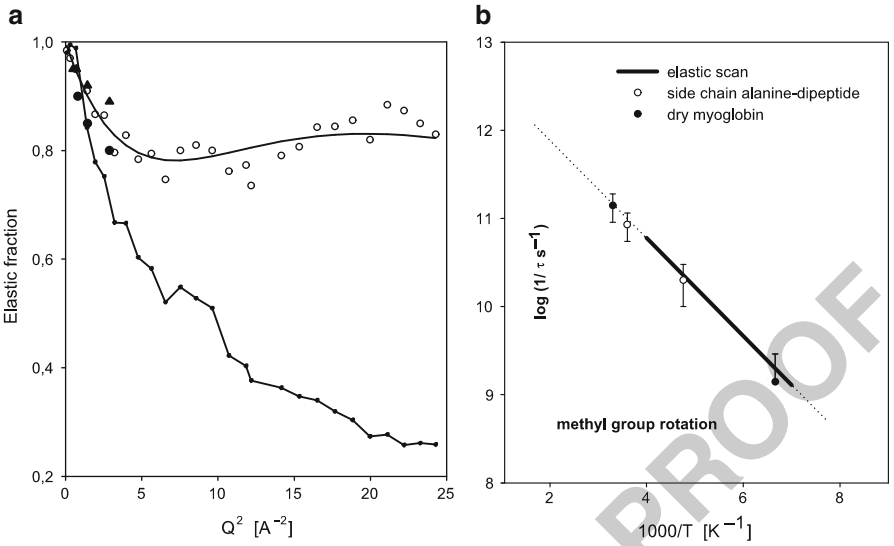

Fig. 8.8 (**a**) Elastic intensity of hydrated myoglobin (IN13) at 300 K, separated into a Gaussian translational component (line with dots) and a non-Gaussian rotational contribution (open circles, IN13, ILL) [4] and and EISF(Q) of methyl group rotation with 25% cross-section (solid line), full circles and triangles: hydrated lysozyme with HFBS according to [22], (**b**) Arrhenius plot of methyl group rotation rates, derived from quasielastic spectra (IN5, Grenoble) with dehydrated myoglobin and alanine dipeptide crystals [21], the full line was derived from elastic scan data (IN13, Grenoble) on alanine dipeptide crystals

A change in temperature shifts the effective time scale of molecular motions with respect to the instrumental window. At low temperature only vibrational motions are resolved, which implies a Gaussian distribution of displacements with a maximum at $r = 0.2\,\AA$.

The maximum broadens slightly when increasing the temperature up to 240 K. Then a distinct shift and a further broadening of the peak occurs. This effect originates from small-scale diffusive motions, which become resolved above 240 K. This feature is absent in dry and vitrified samples and belongs to solvent-coupled or class 2 motions. By contrast,the displacements on a scale of 1.5 $\AA$ are observed in all three environments above 200 K. On such a scale only proton displacements due to rotational jumps are plausible, which is demonstrated in Fig. 8.9. Thus, rotational transitions of side chains, in particular of methyl groups, in the protein interior are not strongly coupled to the properties of the environment [4]. Torsional transitions of methyl groups occur also in solid environments such as molecular crystals. This component, which represents the solid aspect of structural fluctuations, belongs to class 1.

Figure 8.10 shows the temperature evolution of the second moment of the distribution with respect to the three environments. Below 20 K, only zero point vibrations contribute to the displacements $(0.014 \pm 0.003\ \AA^2)$, the vibrational

UNCORRECTED PROOF

Author's Proof

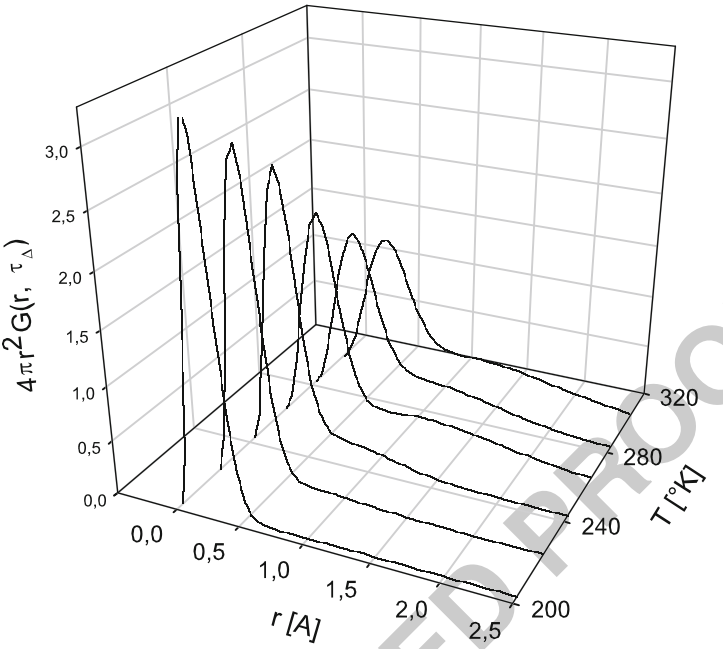

Fig. 8.9 Displacement distribution, $4\pi r^2 G(r,t = 50$ ps), of hydrated myoglobin at fixed time with increasing temperature, peak at r = 0.25 *Å*: vibrational and water-induced librational motions, peak above 1.0 *Å*: side-chain rotational transitions

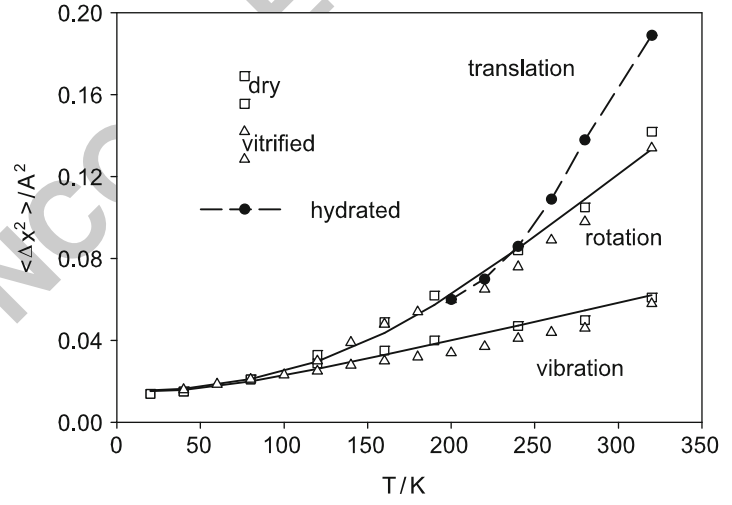

Fig. 8.10 Second moment of the displacement distribution at fixed time in three different environments, vacuum (dehydrated, open squares), vitrified (perdeuterated glucose glass, open triangles) and D_2O-hydrated (0.35 g/g, full circles) using the thermal backscattering spectrometer IN13 at the ILL in Grenoble. The data are corrected for multiple scattering

UNCORRECTED PROOF

Author's Proof

component follows a coth-function with temperature. The displacements of the vitrified sample are slightly lower than those of the hydrated or dry sample. Anharmonic enhancements become significant above 120 K with all three samples, reflecting rotational (class 1) motions of side chains. The onset is gradual and consistent with an Arrhenius temperature dependence of rotational jump rates as shown in Fig. 8.8b. The assignment to methyl group rotation is facilitated by the observation that the class 1 transition is absent in perdeuterated proteins [23]. Water induces additional translational motions of side-chains, which become relevant above $T_\Delta = 240$ K. The onset of water-assisted protein dynamics is abrupt due to a super-Arrhenius temperature dependence of the structural relaxation rate [4,24]. The dynamical transition observed with neutron scattering at $T_\Delta = 240$ K for the non-exchangeable protein hydrogens should be compared with the onset of the heme displacements in fig. 6a at $T_\Delta = 210$ K in myoglobin crystals. The solvent is water in both cases. Apart from different reporter groups, the spatial scale and the time scale probed by the two methods are quite different. Mössbauer spectroscopy is sensitive to small-amplitude motions of the heme iron, the effective wavevector is $Q = 7.2\ \AA^{-1}$, which are faster than about 1 μs. With the neutron back-scattering spectrometer IN13 $Q_{max} = 5\ \AA^{-1}$, and only motions faster than 200 ps are resolved. Assuming that both methods record the same type of solvent-coupled (class 2) fluctuations, the difference in T_Δ can be attributed to the different time windows. With neutron scattering, one can clearly detect class 1 motions in proteins: internal processes such as ligand migration between cavities are most likely assisted by rotational transitions of side chains.

Class 2 motions apply to lateral motions of the heme in its cleft (Fig. 8.1), water-coupled librations of side chains and ligand entry and exit transitions. One important result of the analysis of the hydrogen displacement distribution is the identification of two distinct molecular processes, associated with rotational transitions and translational–librational motion of side chains. Only the latter depend on the solvent. Another important result is that the corresponding correlation functions are not additive, instead their composition is a product of the following form:

$$I(Q,t) = I_{\mathrm{rot}}(Q,t) \cdot I_{\mathrm{trans}}(Q,t,\eta_s) \tag{8.11}$$

The heterogeneity of dynamics sites can lead to a sum of Gaussian displacement distributions, which may account for the observed non-Gaussian shape of the EISF(Q). However the non-Gaussian Q dependence persists in the dehydrated case, when the translational component is arrested. The non-Gaussian nature of the dynamic process, which is active also in the dry state, is thus intrinsic. Transitions between distinct sites, such as rotational transitions, are intrinsically non-Gaussian [4]. The addition of water to myoglobin leads to a further decrease in the elastic scattering function (Fig. 8.7 at 300 K), by enhancing the Gaussian factor. Thus only the Gaussian displacements increase due to class 2 motions. This is very different from just adding another process due to a heterogeneity of reporter groups. This striking result suggests, that a dominant single reporter group exists for neutron scattering in proteins, which performs two kinds of motions simultaneously, rotation

UNCORRECTED PROOF

Author's Proof

and libration–translation. Since the methyl groups in proteins comprise typically 25–30% of the incoherent neutron cross-section, one arrives at the remarkable result, the neutron scattering spectra of D_2O-hydrated proteins reflect essentially three independent types of motion of the methyl side chains: Vibration, rotation and libration–translation. Only translation is coupled to the solvent (class 2). One could imagine as a plausible model, that the axis of the methyl group moves or the group is translated along with side chain to which it is attached.

8.2.3 *The Dynamical Transition from Elastic Scattering Experiments*

The term "dynamical transition" denotes the abrupt onset of class 2 protein structural displacements, which is observed at T_Δ, depending on the instrumental resolution $\Delta\omega$ [2, 25]. In 1989, two transitions were identified and assigned later to class 1 and class 2. Only the second onset at $T_\Delta = 240$ K depends on the degree of hydration. The first onset of anharmonic motion at $T_\Delta* \approx 160$–180 K persists even with dry or vitrified proteins as Fig. 8.10 shows. This effect was attributed above to class 1 rotational transitions of side chains [4, 25]. In the following, we introduce a concept of the dynamical transition which unambiguously defines T_Δ. We show how dynamic information can be deduced from elastic neutron scattering experiments at a fixed instrumental resolution. A more detailed treatment referred to as "elastic resolution spectroscopy" is presented elsewhere. In this method, the instrumental resolution is varied continuously [26, 27].

Figure 8.11 shows the intermediate scattering function of hydration water of myoglobin. The original data were collected in the frequency domain by subtracting the spectra of H_2O and D_2O-hydrated myoglobin and a subsequent Fourier transform to the time domain [28]. On a short time scale, librational motions of water result in a fast β-process. The second slower decay, the α-process, varies with Q and involves reorientation and translation of water molecules along the protein surface [4, 14]. The time window is limited by the instrumental resolution at $\tau_\Delta \approx 12$–15 ps. At τ_Δ the correlation function has decayed to a finite value depending on the temperature, $I(Q, t = \tau_\Delta) = I_{el}(T)$. For longer times there is no further decay observable due to instrumental limitations. The plateau value beyond τ_Δ appears in the frequency domain as a delta component with elastic amplitude $I_{el}(\tau_\Delta, T)\delta(\omega)$. The respective elastic intensity in Fig. 8.11b exhibits a step-like decrease. The associated "dynamical transition" implies that the structural plasticity coupled to this molecular process is fully available beyond τ_Δ, when I_{el} is sufficiently small, ≈350 K. The term "dynamical transition" is justified only because it refers to a collective structural process, the α-relaxation, which determines the viscosity of the liquid (see 8.4). This is not the case for local processes like rotational transitions of side-chains. Structural arrest on a microscopic scale leads to a macroscopic freezing of the liquid, which turns into a glass. The transition is discontinuous in the

UNCORRECTED PROOF

Author's Proof

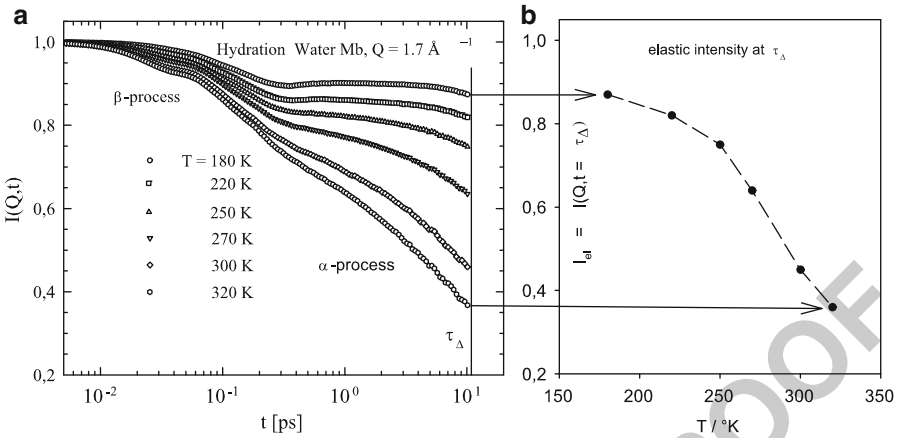

Fig. 8.11 (**a**) Intermediate scattering function of hydration water, I(Q,t), derived by Fourier transforming IN6 time-of-flight spectra of hydrated myoglobin (h = 0.35 g/g) [4, 14], (**b**) Elastic intensity derived from the value of the intermediate scattering function at the instrumental resolution time τ_Δ: $I_{el} = I(Q,t = \tau_\Delta)$

dynamics, but continuous with respect to the molecular structure. It is a dynamical transition, which depends on the relevant experimental time scale. A liquid, if probed on a short enough time scale, looks like a solid even on a macroscopic scale.

Relaxation processes in complex systems are generally non-exponential in time. A very useful model of heterogeneous processes involving a distribution of relaxation times is the Kohlrausch stretched exponential function, which is commonly used to describe dynamics in polymer systems (see for example Chap. 4):

$$\Phi(t) = \exp\left\{-(t/\tau_c)^{\beta}\right\} \tag{8.12}$$

where $\beta \leq 1$ is the stretching parameter.

Figure 8.12a shows this function for $\beta = 1$ (exponential), 0.5 and 0.35. With decreasing β, the decay broadens, involving both fast and slower components compared to the monoexponential case. However, independent of β, the correlation functions coincide at $t = \tau_c$, which defines both the time scale and the characteristic temperature of the dynamical transition. The effect of the instrumental resolution function (dotted line) creates a long-time tail, which will cause further stretching in the high temperature tail of the elastic intensity. The elastic fractions in Fig. 8.12b were derived based on the following assumptions: (1) the correlation time τ_c(T) varies with the temperature according to an Arrhenius law with an activation energy of 17 kJ/mole, a prefactor of 10^{-13}s, and (2) $\tau_\Delta = 2$ ns (for classical reactor backscattering spectrometers like HFBS at NIST, USA, SPHERES at FRMII, Germany or IN16 at the ILL in France). All curves coincide at T_Δ independent of β at $I_{el} = 0.368$, while the onset temperatures are quite different.

UNCORRECTED PROOF

Author's Proof

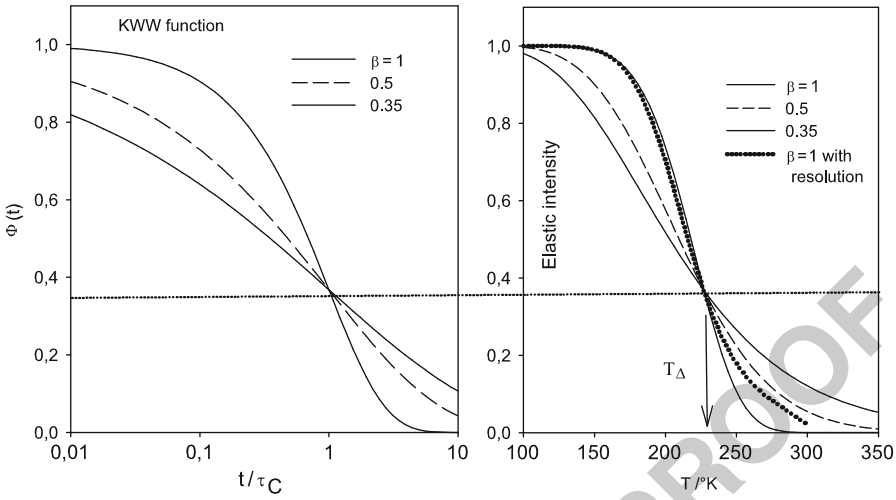

Fig. 8.12 (**a**) correlation function $\Phi(t/\tau_c)$ approximated by a Kohlrausch stretched exponential with three dynamic exponents $\beta = 0.35,\ 0.5,\ 1$. (**b**) Resulting elastic intensity at $\tau_\Delta = 2$ ns, assuming an Arrhenius law for $\tau_c(T) = A \cdot \exp(E_a/RT)$ with $E_a = 17$ kJ/mol and a prefactor $A = 10^{-13}$ s. The effect of a Gaussian instrumental resolution is also shown for $\beta = 1$ (dotted line). The arrow indicates the location of the dynamical transition temperature T_Δ at $\tau_\Delta = \tau_c$, independent of β

The dynamical transition temperature is thus defined by T_Δ, where $\tau_c = \tau_\Delta$ and not by the low temperature deviation from harmonic behavior. The relaxation rates of glass-forming liquids, like those shown in Fig. 8.4, display a super-Arrhenius temperature dependence, which is phenomenologically characterized by a Vogel-Fulcher-Tamman law (VFT):

$$\tau_c^{-1} = \tau_0^{-1} \cdot \exp\{(-H/(T - T_0))\}, \tag{8.13}$$

where τ_0^{-1} denotes a prefactor. H is the high-temperature activation energy [in K] and T_0 denotes a critical temperature, where the correlation time reaches infinity. The parameters of VFT-fit are given in [13].

In the context of the ligand transfer rates of Fig. 8.5, it was mentioned that solvent-coupled protein processes are generally slower than solvent relaxation rates due to protein-intrinsic barriers. Also we have emphasized that the viscosity near the protein surface can differ drastically from the bulk value. In the limiting case that the relaxation rate of the bulk solvent coincides with the protein relaxation rate $\tau_c \approx \tau_s$, we can deduce from the data in Fig. 8.4 a corresponding dynamical transition at a given instrumental resolution τ_Δ. This is shown in Fig. 8.13. For β, we adopt the plausible value of 0.5 and we ignore the slight distortions resulting from the shape of the resolution function (see Fig. 8.12a). The curves refer to an elastic resolution of 2 ns except if indicated otherwise. The dynamical transition onsets

UNCORRECTED PROOF

Author's Proof

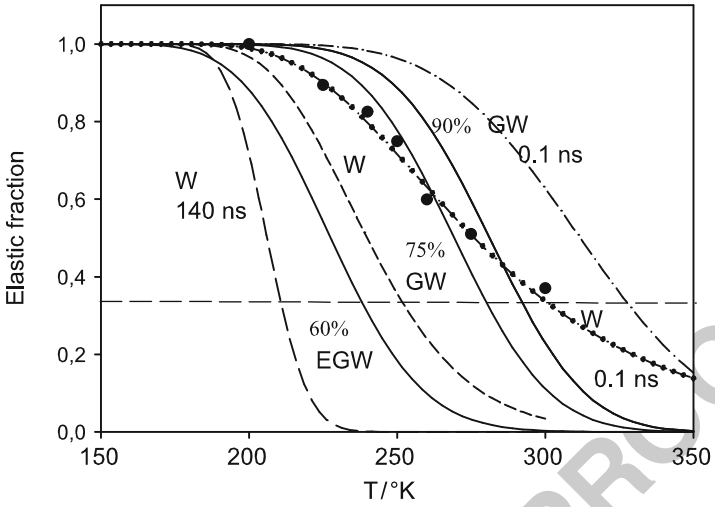

Fig. 8.13 Calculated elastic fraction according to (8.15) and (8.16) using the data in Fig. 8.4. It was assumed that $\tau_c(T) = \tau_s$ for all solvents. T_Δ is defined by the dashed line crossing $I_{el}(T)$. The instrumental resolution was set to $\tau_\Delta = 2$ ns, except if indicated otherwise, the full circles refer to elastic neutron scattering experiments with hydrated lysozyme, $\tau_s = 0.1$ ns [29]

occur in the observed temperature range, 200–300 K. The dashed line indicates our new definition of T_Δ. Hydrated myoglobin and myoglobin crystals, observed with Mössbauer spectroscopy at $\tau_\Delta = 140$ ns, exhibits the lowest onset temperature of 200 K. This is quite close to the observed onset, around 200–210 K in Fig. 8.6. While the onset is quite sharp, the transition itself is significantly broader than the calculated one. Also shown is water as the solvent at a resolution of 0.1 ns superimposed with data on hydrated lysozyme, which fits quite well [29]. However, very similar results were obtained with lysozyme in 90–100% glycerol at 0.1 ns, which should be shifted to higher temperatures. This would suggest a lower effective viscosity near the surface than in the bulk. Such a comparison can provide dynamic information about the state of the solvent near the protein surface.

To analyse real data one has to account for the vibrational Debye–Waller factor and the EISF(Q) of the relevant process corrected for the finite resolution.

Instead of considering the elastic intensities, it is more popular to focus on a derived quantity, the atomic mean square displacements. In [30], a phenomenological relationship between apparent mean square displacements and the bulk solvent viscosity η_b was suggested:

$$\langle \Delta x^2 \rangle_{app} \approx 1/\log(\eta_b) \tag{8.14}$$

Neither the EISF nor the instrumental resolution were explicitly taken into account. With the analysis based on (8.15) and (8.16), we can test this relationship starting

UNCORRECTED PROOF

Author's Proof

from the intermediate scattering function of (8.12). For this purpose, it is sufficient to consider the low-Q range, since the displacements were derived assuming a Gaussian approximation. Second, we are essentially interested in the onset of anharmonic motion. This is the regime, where the structural relaxation time is still smaller than τ_Δ, typically by a factor of 5 [4]. Expanding both, the Gaussian EISF(Q) at small Q is then:

$$EISF(Q \to 0) \approx 1 - Q^2 \cdot \langle \Delta x \rangle_{\text{trans}} \tag{8.15}$$

and the stretched exponential at $t = \tau_\Delta \ll \tau_c$ yields:

$$\Phi(t = \tau_\Delta) \approx 1 - \left(\frac{\tau_\Delta}{\tau_c}\right)^\beta \tag{8.16}$$

which together with:

$$I(Q \to 0, t = \tau_\Delta) \approx 1 - Q^2 \left\langle \Delta x^2(\tau_\Delta) \right\rangle \tag{8.17}$$

yields:

$$\left\langle \Delta x^2 \right\rangle_{\tau_\Delta} \approx \left\langle \Delta x^2_{\text{trans}} \right\rangle \left(\frac{\tau_\Delta}{\tau_c}\right)^\beta = \frac{C}{\eta^\beta} \tag{8.18}$$

The second equality of (8.21) assumes the Maxwell relation between solvent relaxation rate and bulk viscosity: $\tau_c \propto \eta$. Equation 8.21 is certainly quite different from the one proposed above with equ. (8.17) [30].

Figure 8.14 shows the analysis of real elastic scattering data in the present context. To emphasize the contribution of water, a perdeuterated protein phycocyanin, hydrated with 0.3 g/g H_2O was investigated with the back-scattering spectrometer SPHERES at $\tau_\Delta \approx 2$ ns [31]. The data are roughly compatible with the dashed line (W) in Fig. 8.13. A complete analysis requires to account for the harmonic component as well as for the EISF(Q), the step height of the transition. At $T_\Delta = 255$ K, the correlation time of water τ_c equals the resolution time $\tau_\Delta \approx 2$ ns. The various curves refer to different values of the exponent β and correspondingly, different activation energies of the assumed Arrhenius law. The full line represents the choice of $\beta = 0.5$, an activation energy of 4000 K (dotted 4200 K) and the preexponential of 10^{-15}s. Assuming $\beta = 0.35$, one obtains instead H = 7600 K and a preexponential of 10^{-22}s. These differences emphasize the important influence of the relaxation time distribution on activation parameters. For a given β, one can derive relevant dynamic information from the transition curve. To investigate I_{el}(Q,T) directly it is better to start with derived mean square displacements.

So far we have only discussed the effect of the main structural relaxation (α) on the elastic scattering intensity. The intermediate scattering function in Fig. 8.11 shows however a two-step decay. The rate of the fast component varies little with temperature and momentum exchange Q. Only its amplitude increases with the

UNCORRECTED PROOF

Author's Proof

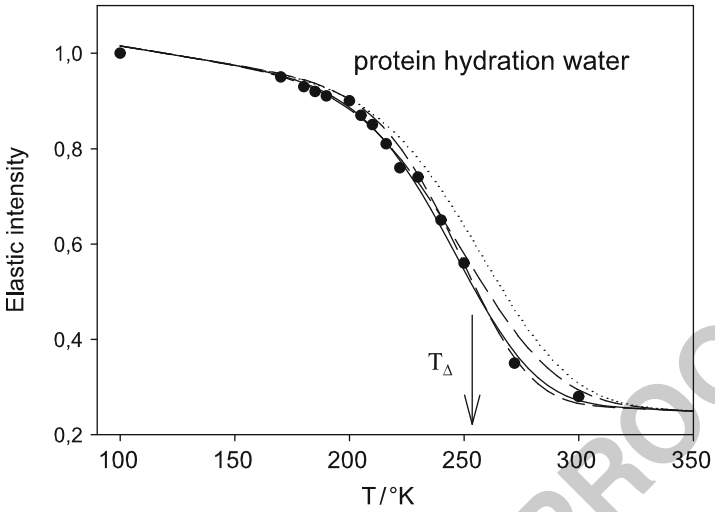

Fig. 8.14 Analysis of elastic neutron scattering data of perdeuterated phycocyanin hydrated with 0.3 g/g H_2O and fits to the stretched exponential model. The value of T_Δ is indicated. The nominal energy resolution was 0.65 μeV and the data refer to $Q = 1.5 Å^{-1}$. The experiment was performed with the back-scattering spectrometer SPHERES at the FRMII facility in Munich [31]

temperature above T_g. To emphasize its local nature, we call it the "fast β-process". The increase of the β-amplitude above T_g gives rise to a first onset in the mean square displacements at about 180 K, which is displayed in Fig. 8.15. Since the β-correlation time ≈1 ps is always shorter than the resolution time of current spectrometers, independent of the temperature, there is no effect of the chosen time window of observation on the apparent displacements. Analysis of high-frequency vibrational spectra of the hydrogen bond network suggests that the β-process originates mainly from fast hydrogen bond fluctuations of water molecules in the cage of nearest neighbours, bonded either to other water molecules or polar protein residues [14]. Figure 8.15 compares the displacements of protein hydration water observed for two time windows of $\tau_\Delta = 2$ ns and 15 ps. The first onset is independent of the instrumental resolution, while the second onset shifts with decreasing time window to higher temperatures. The second onset at T_Δ, originates from collective structural fluctuations giving rise to the α-process. The α-time scale increases strongly with decreasing temperature. This is the reason, why the second onset at T_Δ depends on the observation time scale, τ_{Delta}.

Since protein class 2 displacements are tightly coupled to the water of hydration, protein motions also display a two-step decay in their density correlation function on the same time scale. This two-step scenario was developed in the original analysis of hydrated myoglobin with neutron- time-of-flight and back-scattering spectroscopy [2].

UNCORRECTED PROOF

Author's Proof

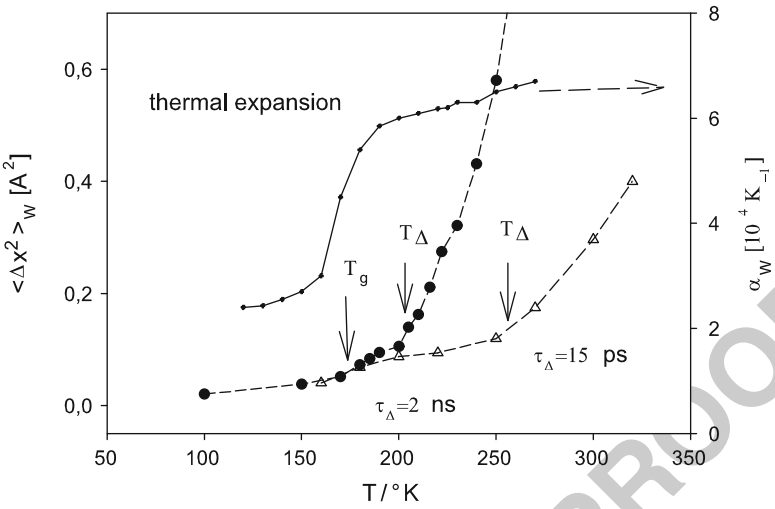

Fig. 8.15 Mean square displacements of protein hydration water from elastic intensities, triangles: myoglobin, data from Fig. 8.11b at 15 ps (time-of-flight spectrometer IN6 at the ILL), circles: perdeuterated c-phycocyanin, H_2O-hydrated, 0.3 g/g at 2 ns (SPHERES, FRMII Munich), and thermal expansion of hydration water (myoglobin) derived from the O-H stretching vibration. The glass temperature T_g and the resolution dependent onset of the α-process, T_Δ are indicated [14,31]

8.2.4 *Conclusion on Protein-Internal Structural Motions and Biological Function*

The main conclusion of the first part of this chapter is the discrimination of class 1 and class 2 processes according to their coupling to the solvent. Intercavity migration of the ligand belongs to class 1 as well as the rotational transition of internal side chains. The ligand transfer across the protein–solvent interface and translational motion of surface side-chains are coupled to the solvent and belong to class 2. The main dynamic coupling parameter is the solvent viscosity at the protein surface η_s which can be different from the bulk value. Even small globular proteins can thus provide a unique chemical environment, which is also dynamically isolated from the solvent. Even though the heme group, the active site of myoglobin, performs translational motions, which are modulated by the external solvent, the binding of the ligand to the heme iron is a class 1 reaction. One of the unsolved puzzles of the field is that the final binding reaction B→A is always polychromatic and independent of the solvent [32].

A distribution of activation enthalpies, reflecting the conformational heterogeneity of the protein structure was invoked, but the molecular origin of the disorder is still obscure. In [5], it was suggested that the sliding motion of the heme in its cleft, modulates the effective force on the heme iron, which is covalently attached to the imidazole side chain of His F8. This effect also modulates the barrier of

UNCORRECTED PROOF

Author's Proof

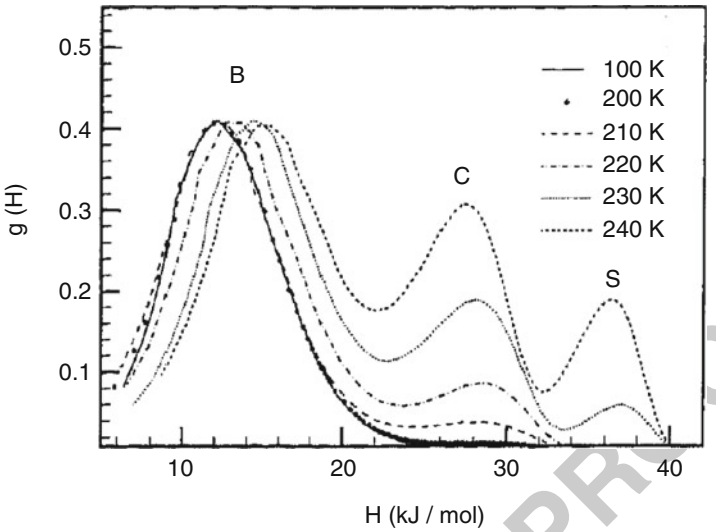

Fig. 8.16 Normalised distribution function of activation energies referring to elementary steps of the CO-binding kinetics to horse myoglobin. B, C and S denote the partial enthalpy distributions of rebinding from the respective docking sites to final state A according to the four state model and Fig. 8.1 [13]

UNCORRECTED PROOF

B→A when the covalent bond between heme iron and CO is formed. If the crossing of the barrier at the heme site occurs on a time scale that is faster than the visco-elastic sliding, an apparent static distribution of barrier heights will result. The above analysis indicates, that the structural relaxation of the solvent is the main factor that determines the rate of heme sliding. It follows that the observed barrier distribution should change significantly, when the rate of visco-elastic sliding becomes comparable to the rate of covalent bond formation at the heme iron. In the case of CO-myoglobin in 75% glycerol-water, the crossover takes place between 210 and 220 K, where the solvent relaxation rate $k_s(T)$ becomes comparable to the rebinding rate k_{BA} at about 10^6 s^{-1} (Figs. 8.3 and 8.4). Figure 8.16 shows, that the activation enthalpy spectrum of B→A is constant between 100 and 200 K. However, above 200 K the B-distribution shifts towards higher values, suggesting relaxation to a new product state B*→B [33]. This suggests, that heme sliding does affect the rate of bond formation. However, the distribution does collapse to a delta-function. The C- and S- distributions change in relative weight with respect to B, as a result of the temperature dependent population of kinetic states. In particular the escape fraction N_{out} increases with the temperature above 200 K.

In the second part of the chapter, a more precise definition of the dynamical transition is suggested. We start from the time domain with a distribution of relaxation times and switch to the frequency domain by defining the elastic intensity as the long-time value of the intermediate scattering function limited by the

Author's Proof

resolution of the spectrometer. The dynamical transition is thus defined by the temperature, where the elastic intensity has decreased to its 1/e value. This value is independent of the detailed relaxation time distribution, while the onset temperature is strongly affected by the shape of the spectrum. This concept allows to test various coupling models, for instance whether the solvent relaxation rate τ_s of various solvents equals the protein structural relaxation rate τ_c.

Several misconceptions exist about the nature and the mechanism of the dynamical transition and its relation to the glass transition [14, 25]. It is often claimed that the dynamical transition can be suppressed by vitrifying the protein in a glassy matrix [23**?**]. While class 2 motions can be entirely suppressed at infinite external viscosity, class 1 motions (and the related anharmonic onset) are active irrespective of the environment (see Fig. 8.9). One likely origin of the discrepancy derives from the fact that the glassy matrix dominates the elastic scattering function unless it is perdeuterated. In Figs. 8.7–8.10 a perdeuterated glucose matrix was used. Also the work of Tsai et al. [34] on lysozyme in glycerol (see figure 11.3 in the Chapter of Wood and Weik) is in strong contradiction with Paciaroni et al. [29]. While Tsai et al. derive an onset temperature of 388 K, the onset in 90–100% glycerol occurs at 240 K as Fig. 8.13 shows. The dynamical transition is certainly not related to an energy landscape or a molecular resilience [23]. Instead it reflects the activation energy spectrum of molecular processes probed by a spectrometer on a finite time window. It does not even make sense to ask, what is actually "driving" the dynamical transition, protein motions, rotation or translation of water molecules. There is no driving force, just collective fluctuations of the protein-water system, that will be structurally arrested at the glass transition. The glass transition, which implies by definition the freezing of translational motions on a macroscopic time scale of 100 s, occurs at about 170 K for the protein-water system. At $T_g = T_\Delta(100\ s)$, however the protein-water systems starts to soften due to an increasing amplitude of fast hydrogen bond fluctuations. On a molecular scale, the coupling mechanism between protein and its solvation shell is the hydrogen bond network. A molecular transfer necessitates the simultaneous breaking of several hydrogen bonds. Fluctuations at this basic level may be considered as the main driving force of the dynamical transition [14, 24, 35].

AQ5

8.3 Global Diffusion of Macromolecules

8.3.1 Dynamic Light Scattering of Colloids

As early as 1908 and 1910, with the works of Smoluchovsky and Einstein, respectively, it was clear that density fluctuations in condensed matter lead to local inhomogeneities that could scatter beams. The progress of such studies was slow due to the unavailability of high intensity light beams, until the introduction of the laser at the beginning of 1960s. Then began an intense activity on experimental

UNCORRECTED PROOF

Author's Proof

studies on colloidal systems by dynamical light scattering (DLS) together with theoretical papers aiming at the interpretation of the experimentally measured quantities. Phillies [36, 37] introduced the generalized Stokes–Einstein relaxation that determines the mutual diffusion coefficient measured by DLS:

$$D_m = \frac{(1-\Phi)}{f}\left(\frac{\partial \pi}{\partial c}\right)_{P,T} \tag{8.19}$$

where $\frac{-1}{c}(\partial\pi/\partial c)^{-1}$ is the osmotic compressibility of the solution, Φ the hydrodynamic fraction of the molecules in solution and f is a friction coefficient. This diffusion coefficient being extracted from the pair-correlation function is different in nature from the self-diffusion coefficient measured by, for example, tracer diffusion experiments: D_s. For very low concentrations, the interactions between molecules can be neglected and D_s and D_m are equal to D_o the diffusion coefficient of a unique macromolecule in a solvent (0 refer to zero concentration). D_o given by the Einstein's law : $D_o = k_\mathrm{B}T/f$ where T is the temperature in K, k_B the Boltzmann constant and f is a friction term that Stokes has shown equal to be equal to $6\pi\eta R$ for a sphere of radius R in a continuous solvent of viscosity η. When the concentration of macromolecules in solution increases, the interactions cannot be neglected and $D_\mathrm{m}(\Phi)$ begins to be significantly different to $D_\mathrm{s}(\Phi)$ and D_0. Moreover and adding to the different nature of the diffusion coefficients, one should distinguish between temporal regimes. One usually introduces three time domains: (1) $t \ll \tau_\mathrm{B}$ with τ_B is the time the correlation of the velocity needs to relax, that is, the necessary time to reach a Brownian regime for the macromolecules; (2) for $\tau_\mathrm{B} \ll t \ll \tau_i$ (τ_i) is the time needed by the particle to interact with its neighbors) one defines a short time diffusion coefficient: the macromolecules only experience hydrodynamic interactions; and (3) in the time domain $t \gg \tau_i$, we observe the diffusion of the particle in solution, the hydrodynamic and direct interactions are established and we define a long time diffusion coefficient.

In the short time regime, memory effects can be neglected and the dynamical functions can be expressed as a function of the equilibrium distributions; the theory is now relatively complete [38–40]. Ackerson has derived a relation for the apparent diffusion that can be split into contributions from the direct and hydrodynamic interactions:

$$D = D_0 \frac{H(Q)}{S(Q)} \tag{8.20}$$

Beenakker and Mazur [41, 42] have calculated the hydrodynamic factor, $H(Q)$ for solutions of concentrated hard spheres. In particular, they have shown the characteristic wave vector dependance of $H(Q)$ for different volume fractions Φ. The theoretical predictions for $H(Q,\Phi)$ can be compared to experimental results.

The dependence of the self-diffusion coefficients at short and long times, D_s^s and D_s^L, on the volume fraction, cannot be calculated exactly, but several

UNCORRECTED PROOF

Author's Proof

theoretical approximations have been introduced. Some authors have decoupled the contribution from hydrodynamic and direct interactions, as Beenakker and Mazur [41, 42]. Médina–Noyola [43] introduced a way of calculating D_s^L from D_s^s and the structure factor S(Q) of the solution. Tokuyama and Oppenheim [44] have developed a more systematic way of calculating D_s^s and D_s^L that includes both hydrodynamic and direct interactions for hard sphere solutions.

The structure of charged particles in solution was studied theoretically by Hayter and Penfold [45], who derived an analytical structure factor for charged spheres interacting with a screened electrostatic potential. This theory (Mean Spherical Approximation) can be applied at rather small global macromolecular charges if the particle concentration is not too high, and if the contribution of counterions to the scattered intensity can be neglected. The latter only affects the screening of the Coulombic potential by reducing the Debye length. The potential no longer decreases with 1/r but rather with a Yukawa-type function. Hansen and Hayter [46] introduced a renormalization method of the effective radius of the particle in order to extend the theory to low concentration of highly charged colloids. In such a case the contact potential is much higher than k_BT, and thus the contact probability of the particles is almost zero $g(r > 2a) \simeq 0$. The hard sphere potential doesn't play a physical role. Their method involves rescaling the radius of the particle. Finally in 1986, Belloni [47] included the colloidal concentration in the calculation of the Debye length and thus the screening of the electrostatic forces.

8.3.2 *Protein Structure Factor and Diffusion*

The cytoplasm topology directly influences protein diffusion. Beyond transport mechanisms, the kinetics of a biochemical reaction will be affected by the mobility reduction, which can become diffusion limited inside the complex interior of cells. The transport inside cells can generally be divided into three types :

1. The active transport which requires energy (ATP hydrolysis).
2. Simple diffusion (or Brownian) in which the mean-square displacement of the molecules is a linear function of time : $\langle r^2 \rangle \simeq Dt$.
3. Anomalous diffusion, in contrast to simple diffusion, in which the mean-square displacement of the molecules is NOT a linear function of the time : $\langle r^2 \rangle \simeq Dt^\alpha$. It can be subdiffusive ($\alpha < 1$) and superdiffusive ($\alpha > 1$), the former being mostly encountered in cells.

It is now widely accepted that the dominant mechanism is diffusion [48] (non-active transport), although there is one group suggesting a combined transport in the nucleus [49]. The nature of the diffusion process (Brownian or non-Brownian) still remains a matter of discussion. In what follows, only diffusive transport will be discussed because neutron scattering is probably less suited for studying activated transport.

UNCORRECTED PROOF

Author's Proof

The motion of a particle, at infinite dilution and in the absence of field, can be described by a random walk, which leads to:

$$\langle r^2 \rangle = 6D_o t, \tag{8.21}$$

where $\langle r^2 \rangle$ is the mean square displacement of the particle during a time τ. The presence of other macromolecules in the cytoplasm will strongly modify the value of D_o, which is dependent on the excluded volume (the space which is physically not accessible to the center of mass molecule due to the presence of others). For a total macromolecular volume fraction Φ of the order of that present in the cytoplasm ($\Phi \simeq 0.3 - 0.4$), the diffusion coefficient $D_s(\Phi)$ can be reduced by more than one order of magnitude. A significant number of experimental and theoretical studies aim to measure and understand the mechanisms that lead to the reduction in $D_s(\Phi)$. As mentioned before, this problem is very complex because one single diffusion coefficient at infinite dilution is replaced by a number of different ones at higher crowding fractions.

The discovery of fluorescence proteins, such as the Green Fluorescence protein AQ6 [**?**], together with improvements in imaging technology, has allowed the study of protein diffusion inside cells. Fluorescence techniques [50] like FRAP [51] (fluorescence recovery after photobleaching), FRET (fluorescence resonance by energy transfer) and FCS (fluorescence correlation spectroscopy), complement those usually used to study molecular diffusion (DLS, NMR, tracer methods ..) in vivo. All these methods probe the diffusion of molecules over distances typically of the order of the cell size or smaller, but in any case much higher than the inter molecular distances. In contrast, neutron scattering allows the study of interactions and molecular motions over typical protein–protein distances in protein solutions and in cells. Thus, we can test models developed to describe the statics and dynamics of micellar and colloidal suspensions. These objects generally have a size significantly higher than proteins where the first interaction peak can be probed by light scattering.

8.3.3 Protein Structure Factor

Proteins in solution with their well-defined tertiary structure provide an excellent model system to study the interaction of simple charged molecules. Polydispersity arises only from protein aggregation and not from distributions in particle size. For some proteins, aggregates can be avoided under certain biochemical conditions or eliminated by centrifugation of the solution.

The first attempt to study the structure and interparticle interactions in protein solutions using the analysis of Hayter and Penfold [45] was performed on Bovine Serum Albumin (BSA) in 1983 [52]. BSA is a prolate ellipsoidal-shape protein (a,b,b) with a = 70 Å and b = 20 Å, thus the analysis of the data were performed using a form factor of an ellipsoid with a structure factor calculated for equivalent

UNCORRECTED PROOF

Author's Proof

charged hard sphere. Later the same analysis was performed on hemoglobin inside red cells [53] and in solution [54], a protein that has a nearly spherical shape and therefore leads to more satisfactory results.

Hayter and Penfold [45] calculated the structure factor of a colloidal solution that experiences an interaction potential composed of a hard sphere part plus an electrostatic tail using the Mean Spherical Approximation (MSA). Mathematically, the electrostic tail follows a Yukawa-type function $\beta V(r) = V_{ij}(2r_0)2r_0\frac{e^{-\kappa(r-2r_0)}}{r}$ for $r > 2r_0$ and $V(r) = \infty$ for $r < 2r_0$. $\beta = 1/k_BT$ and $V_{ij}(2r_0)$ is the contact potential which depends on the global protein charge Z_p. κ is the inverse of the Debye length L_D, which reflects the screening of the potential due to counterions in solutions.

The neutron scattered intensity by a solution of monodisperse macromolecules in solution with a spherical symmetry can be described

$$I(q) = \Phi v_0(\Delta\rho)^2F^2(Q).S(Q), \tag{8.22}$$

where Φ is the volume fraction occupied by the macromolecules, v_0 their volume, $\Delta\rho$ is the scattering length density difference between the solvent and the macromolecules (in cm^{-2}), F(Q) is the form factor of the particle and S(Q) denotes the interparticle structure factor. The form factor of the protein can be measured at very low concentration where $S(q)\sim1$, and it is then possible to access to the structure factor by a simple division of the scattered spectra by the form factor at each protein volume fraction. The spectra are then refined using the calculated structure factor of Hayter and Penfold [45] or with the corrections introduced by Belloni [47]. The free parameters of the refinements are the volume fraction Φ, the radius of the protein r_0 and the net protein charge Z_p. The Debye length is generally computed from the ionic strength of the solution and is implemented in the model. For myoglobin solutions [55] one gets $r_0 \simeq 16$ Å and $Z_p \simeq 2e$ for each volume fraction, the radius is a little bit smaller than the real hard sphere radius of the protein but the small charge is compatible with the fact that the protein is at high concentration and will impose the pH of the solution close to its isoletric point.

For hemoglobin solutions [53, 54] the experimental results can be satisfactory compared to theoretical calculations, although the volume fraction extracted from the analysis is slightly lower than the real ones, which has been interpreted as being due to the limited aggregation of the hemoglobin tetramers in solution.

UNCORRECTED PROOF

8.3.4 *Protein Diffusion as a Function of the Concentration*

The first step to understanding the physical mechanism that leads to the mobility reduction in crowded media is to look at the evolution of the diffusion coefficient of a protein solution of as a function of the concentration. Riveros-Moreno and Wittenberg have measured the concentration dependence of the self-diffusion coefficient in myoglobin and hemoglobin solutions [56] up to volume fractions

Author's Proof

of $\Phi \simeq 0.2$ and $\Phi \simeq 0.26$, respectively. They found, a plateau at low protein concentration followed by an exponential decrease of D_s down to more than one order of magnitude at higher protein concentration. Alpert and Banks [57] showed that the mutual diffusion coefficient D_m, measured by dynamical light scattering, has a much weaker dependance then the self-diffusion coefficient D_s. This was soon confirmed by Hall et al. [58] who compared the self- and the mutual-diffusion coefficient evolution as a function of the concentration in hemoglobin solutions. The self-diffusion coefficients are long-time ones because the techniques used for the measurements probe the diffusion process over much longer than the intermolecular ones.

The analysis of the diffusion properties of proteins using a combined approach by SANS or small-angle X-rays scattering (SAXS) to get the structure factor, and neutron spin-echo spectroscopy (NSE) to obtain the apparent diffusion coefficient has been performed by different authors. On the one hand, myoglobin and hemoglobin solutions were studied [3, 4, 55, 59, 60] motivated by the aim to understand whether protein dynamics could be described by models developed for colloids and if protein diffusion can assist oxygen diffusion. On the other hand, experiments were performed on Ferritin solutions, to study the dynamics at high concentrations where paracrystalline order occurs [61, 62], to study the hydrodynamic interactions in perfectly monodisperse spherical macromolecular solutions [63], or more recently to study diffusive dynamics in solution [64].

Neutron spin echo spectroscopy gives access to full intermediate scattering function $S(Q,t)$:

$$S(\mathbf{Q},t) = \frac{1}{N}\left\langle \sum_{i,j}^{N} b_i b_j e^{-i\mathbf{Q}.[\mathbf{r}_i(0)-\mathbf{r}_j(t)]} \right\rangle, \tag{8.23}$$

where i and j run over all the scattering centers N, of respective scattering lengths b_i and b_j and position $r_i(0)$ at time $t = 0$ and $r_j(t)$ at time t. In the wave vector range $2\pi/Q \gg d$ (where d is the average distance between two scattering centers), usually referred to as the small angle limit, the intermediate scattering function of a solution of almost spherical macromolecules in solution, reads:

$$\frac{S(Q,t)}{\Phi v_p (\Delta\rho)^2 F^2(Q)} \simeq \frac{1}{N'}\left\langle \sum_{i,j}^{N'} e^{-i\mathbf{Q}.[\mathbf{r}_i(0)-\mathbf{r}_j(t)]} \right\rangle \tag{8.24}$$

where Φ is the volume fraction occupied by macromolecules of volume v_p, i and j run over all the molecule centers N' whose positions are $r_i(0)$ at time $t = 0$ and $r_j(t)$ at time t, respectively. F(q) is the form factor and $\Delta\rho$ is the scattering length density contrast between the macromolecules and the solvent. The normalized intermediate scattering function $I(Q,t) = \frac{S(Q,t)}{S(Q)}$ obtained for myoglobin solutions are presented in Fig. 8.17.

UNCORRECTED PROOF

Author's Proof

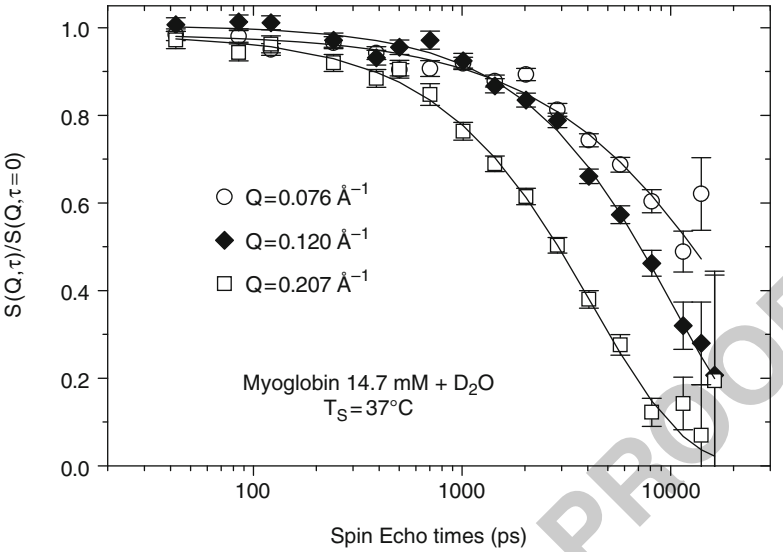

Fig. 8.17 Intermediate scattering function I(q,t) measured on the spin echo spectrometer G_1bis (Laboratoire Léon Brillouin, Saclay, France) on myoglobin solution of protein volume fraction $\Phi \simeq 0.2$

There is no significant departure from a single relaxation decay whatever the concentration of the solution. We can consequently extract a wavevector-dependent diffusion coefficient by refining the curves using the relation:

$$I(Q,t) \sim e^{-D(Q)Q^2 t}. \tag{8.25}$$

Figure 8.18 shows the evolution of the apparent diffusion coefficient $D(Q)$ as a function of the wave vector for three different protein concentrations. Independent of protein concentration, the wave vector evolution of $D(Q)$ is similar, an increase at low-wave vector and a plateau at high Q. The extrapolation of $D(Q)$ to $Q = 0$ leads to the mutual diffusion coefficient measured by light scattering D_m, whereas the value of the plateau corresponds to a self-diffusion coefficient D_s. The plateau is observed in the wave vector range where $S(Q) \sim 1$ which generally corresponds to the incoherent approximation of coherent scattering. In this Q range, a small change in the position of the proteins, $\mathbf{r}_i(0) - \mathbf{r}_j(t)$ will induce a strong variation of the phase term $\mathbf{Q}.[\mathbf{r}_i(0) - \mathbf{r}_j(t)]$ and the cross term $i \neq j$ of (8.24) will vanish leaving only the self-correlation term.

8.3.4.1 Concentration Dependance of the Self-Diffusion Coefficient

The concentration dependence of the self-diffusion coefficient $D_s(\Phi)$ obtained for a myoglobin solution is shown in Fig. 8.19. The theoretical calculation by Tokuyama and Oppenheim [44] for the short- and the long-time self-diffusions for a hard sphere solution are also shown in the figure.

UNCORRECTED PROOF

Author's Proof

this figure will be printed in b/w

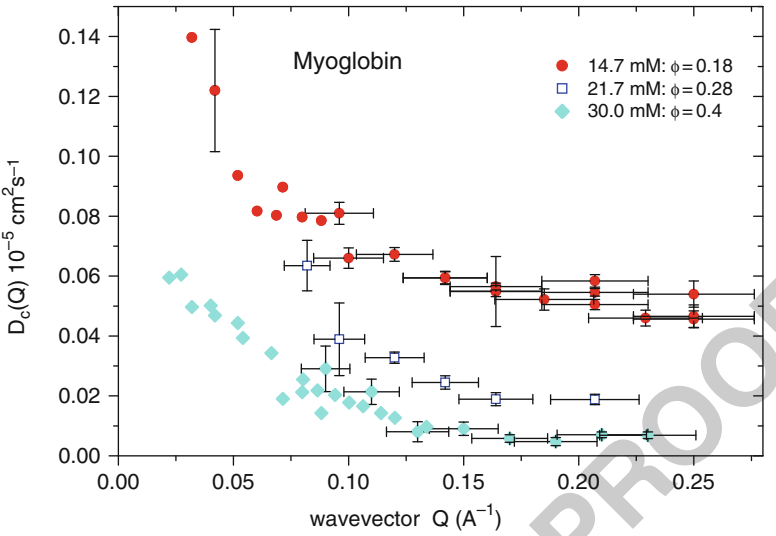

Fig. 8.18 Apparent diffusion coefficient measured on myoglobin solution of protein volume fraction ranging from $\Phi \simeq 0.18$ to $\Phi \simeq 0.4$

UNCORRECTED PROOF

For globular proteins like myoglobin, the Brownian time can be estimated using $\tau_B \simeq \frac{M}{f} = \frac{M}{N}\frac{D_o}{k_B T} \simeq 10$ ps. The interaction time can be estimated in one of two ways: (1) some authors [65] define it as the time necessary to diffuse by a distance equal to its own hydrodynamic radius such that $\tau_i \simeq \frac{a^2}{D_o} \simeq 30$ ns, where a is the hydrodynamic radius of the protein. This calculation, which is not dependent on the quantity of protein in solution, holds for moderate concentrations but can differ significantly at high values of Φ; (2) assume that it corresponds to the time necessary to diffuse over the mean surface to surface distance of two proteins, which is clearly concentration dependent. Thus $\tau_i \simeq 2\frac{d^2}{D_o}$ with $d = a\left(\frac{4\pi}{3\Phi}^{1/3} - 2\right)$. This leads for $\Phi \simeq 0.2$ an interaction time $\tau_i \simeq 34$ ns very similar to the first estimation, but decreases down to $\tau_i \simeq 1$ ns for $\Phi \simeq 0.4$. Nevertheless, this interaction time remains a rather crude approximation, because, for example, the diffusion coefficient which is used for the calculation should not be the infinite dilution one D_o but rather the short time one which depends on the concentration. The relaxation times measured in myoglobin solutions extracted from the Fig. 8.17 are of the order of 1 ns, which falls in between the Brownian and the interaction time. The measured diffusion coefficient should consequently experience only hydrodynamic interactions. Under these conditions, it is a short time diffusion coefficient ${}^{s}D_s(\Phi)$. In Fig. 8.19 the refinement of the diffusion coefficients measured by tracer methods [66], which by definition corresponds to the long time limit, is represented by a continuous black line. The correspondence between our NSE data and the value ${}^{l}D_s(\Phi)$ is rather good. To understand which type of diffusion coefficient we are indeed measuring (short- or long- time), it is interesting to compare the theoretical results. Also added

Author's Proof

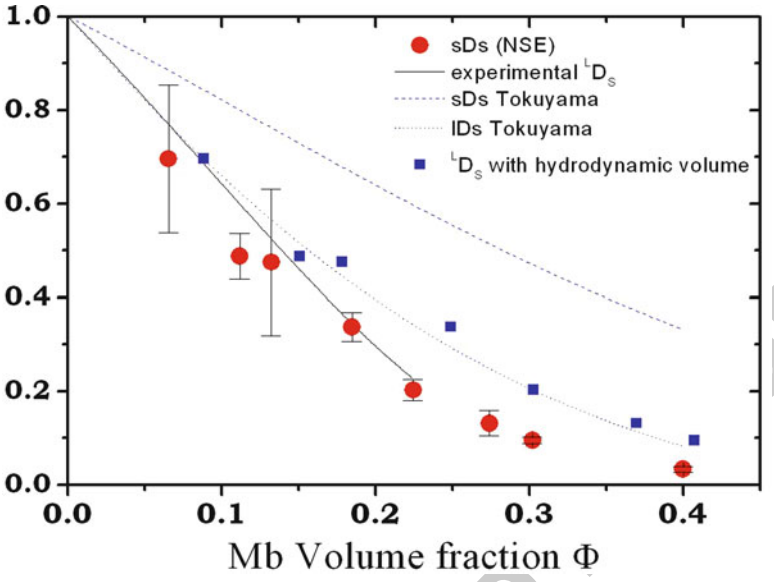

this figure will be printed in b/w

Fig. 8.19 Self-diffusion diffusion coefficients of myogoblin solutions measured by neutron spin-echo of myoglobin solutions as a function of the concentration (Full circle), best refinement of the long-time self diffusion coefficient measured by tracer methods (full line), theoretical calculation for short- (dot) and long-time self diffusion coefficient obtained by Tokuyama and Oppenhein [44]. The full squares are the neutron spin echo results after including the water hydration shell in the calculation of the hydrodynamic volume (see text)

UNCORRECTED PROOF

in figure 8.19 are the results of the computation of Tokuyama and Oppenheim [44] for the short- and the long-time diffusion coefficients for hard sphere solutions. Our results together with the ones obtained by tracer methods are significantly lower than the theoretical predictions also for the long-time diffusion coefficient. In what follows, we try to explain this discrepancy. In 1977, Ross and Minton [67] noticed the need to include the volume of the hydration water shell in the computation of the hydrodynamic volume, in order to describe the viscosity of hemoglobin solutions by a hard quasi-spherical model. To compute the volume fraction on Fig. 8.19, we used the protein concentration (determined with a high precision by UV absorption) and the specific volume of the protein as $v_p \simeq 0.741$ cm^3.g^{-1}: this corresponds to the dry volume fraction of the protein. The full squares in Fig. 8.19 are the spin echo results where the dry volume was replaced by the hydrodynamic one by using $\Phi_h = c_p v_h$ with $v_h = v_d + \delta v_s$. v_s is the specific volume of the solvent and δ ($0 \leq \delta \leq 1$) is the weight fraction of the hydration shell contributing to the volume, which is commonly assumed to be $\delta = 0.35$. There is a quite good agreement between the experimental results and the calculation of Tokuyama and Oppenheim [44] for the long-time diffusion coefficient for hard sphere solutions, which supports the idea that the self-diffusion coefficient measured by spin echo is a long-time one.

AQ7

Author's Proof

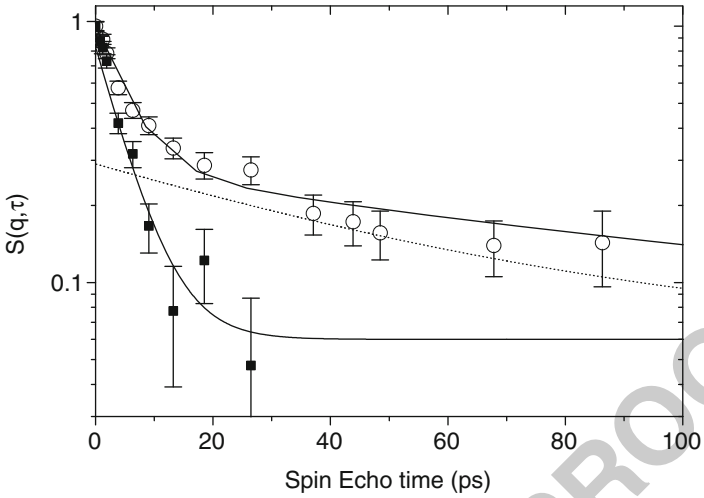

Fig. 8.20 Intermediate scattering function $I(Q = 1\,\text{Å}^{-1}, t)$ measured on the spin echo spectrometer $G_1 bis$ (Laboratoire Léon Brillouin, Saclay, France) on hemoglobin solution of protein volume fraction $\Phi \simeq 0.25$ (circle) and on water (square). The contribution of the protein is proportional to its ratio of protons in solution and is represented as the dot curve

8.3.4.2 Search for the Short-Time Diffusion Coefficient

In hard sphere suspensions at high volume fraction ($\Phi \simeq 0.4$), it was shown by the time evolution of the mean square displacement that particles typically achieve their asymptotic long time behaviour after diffusing over distances equal to only a few tenths of its diameter [68, 69]. In protein solutions, at slightly lower concentration (350 mg.ml^{-1}), one expects to observe the transition from long-time to small-time behaviour at high wavevectors. the mixture of coherent and spin incoherent scattering leads to a strong decrease of the scattered beam polarisation, which is highly unfavourable for NSE measurements. Therefore, such measurements must be performed on fully incoherent samples (H-protein in H_2O). Figure 8.20 shows the intermediate scattering function of a hemoglobin solution ($\Phi \simeq 0.25$) and that of pure water at $q = 1\,\text{Å}^{-1}$. The protein contribution is proportional to the ratio of the number of hydrogens in the protein with respect to the total number in solution, which can be estimated around $\simeq 25\%$. A clear signature of the protein can be separated from the water contribution, which is represented by the dotted curve. The apparent diffusion, which can be extracted from the signal is $D_{\text{mes}}^{\text{app}} = 14.9(\pm 3) * 10^{-7}\,\text{cm}^2\text{s}^{-1}$, and is more than twice the Stokes–Einstein one at low concentration, which should normally be the highest limit for both D_s^L and D_s^S. It is thus necessary to introduce an additional dynamical phenomenon to explain this relaxation time. Proteins undergo aleatory rotational motions, referred to as rotational Brownian motions which are similar in nature to the translation ones. Their physical origin is an aleatory torque which results from unbalanced collisions

UNCORRECTED PROOF

Author's Proof

of the solvent molecules with the protein. At high momentum transfer, these motions will contribute to the translational one as an additional term $\tilde{D}^r \simeq R_g^2 D_r$. Taking the values given in the literature [70] and assuming that for a solution of concentration $\sim 350\,\mathrm{mg.ml^{-1}}$ one gets $D_s^s \simeq D_s^0/2$ (corresponds to the theoretical predictions), we get a new apparent diffusion coefficient $D^{\mathrm{app}} = \tilde{D}^r_{rbc} + D_s \simeq 6.2 * 10^{-7}\,\mathrm{cm^2.s^{-1}}$ which remains much below the measured one. Thuis the relaxation phenomena which are measured by NSE probably differ in nature from a Brownian motion. Most likely this effect originates from internal motions of the protein [71].

8.3.4.3 Wave Vector Dependence of $D(Q)$

As was seen in Fig. 8.18, the wavevector dependence of the apparent diffusion coefficient is always the same whatever the protein concentration is solution. This behaviour is characteristic of the collective nature of $D(Q)$. In molecular liquids the interactions arise from direct forces. In 1959, P.-G. de Gennes calculated a relationship between the second moments of the coherent and incoherent scattering peaks [72] : $\omega^2_{\mathrm{coh}} = \omega^2_{\mathrm{inc}}/S(Q)$. In colloidal or protein solutions, we have to account for additional interactions mediated by the solvent namely the hydrodynamic interactions, which appear in relation 8.3.1. In the limit of zero scattering wave vector, this value must lead to the one measured by light scattering. It is weakly dependent on the protein concentration because the increase of the friction value is partially compensated by the strong variation of the osmotic compressibility. When the scattering wave vector increases, the structure factor increases, which accounts for the decrease of $D(Q)$. Formally equation 8.3.1 is only valid in the limit of short times, when the neighboring molecules can be considered as immobile. This means that the diffusion coefficient is the one measured at short times. But we have shown that we only have access to the long-time diffusion coefficient D_s^{L}, and not D_s^{S}, which would exclude any possibility to compute the hydrodynamic factor $H(Q)$. The top panel in figure 8.21 plots the product $D(Q) * S(Q)/D_o$ deduced from the neutron scattering data. In accordance with the theoretical predictions for $H(Q)$ [42], this product oscillates in phase with the structure factor, and after renormalisation by a constant in order to account for the difference between the short- and long-time diffusion coefficient the agreement between experimental results and theoretical results is satisfactory. P. Segrè and P. Pusey showed a similar relation between the short- and long-time apparent diffusion coefficient, $D^{\mathrm{S}}(Q)$ and $D^{\mathrm{L}}(Q)$, in colloidal suspensions up to volume fractions of 30% [**?**]. This observation has currently no theoretical explanation, but Fig. 8.21 tends to indicate a strong contribution of hydrodynamic interactions in protein mobility.

AQ8

8.3.4.4 Measurements Inside Cells

The measurement of hemoglobin diffusion inside red blood cells (RBC) is not straightforward. Dynamic light scattering is dominated by membrane fluctuations

UNCORRECTED PROOF

Author's Proof

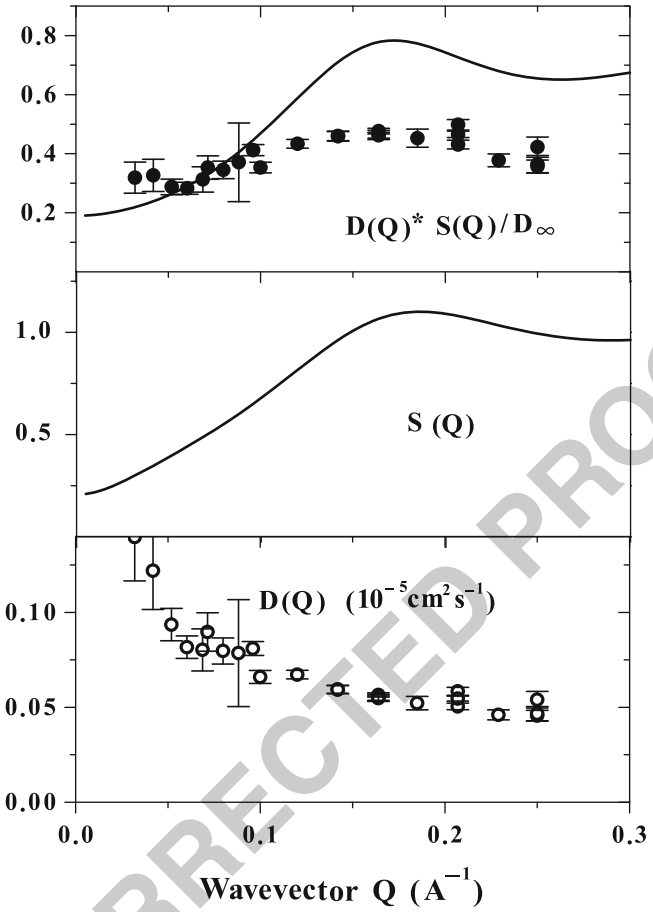

Fig. 8.21 Apparent diffusion coefficient, structure factor and product $D(Q) * S(Q)/D_o$ obtained for myoglobin solution at a concentration of 14.7 mM ($\Phi \simeq 0.2$)

UNCORRECTED PROOF

[73], whereas NMR measures protein motions over hundred of nanometers where cell confinement effects can become important [74, 75]. Krueger an Nossal [53] have used neutron scattering to study the structure factor of hemoglobin solutions inside red blood cells. They have especially shown, using contrast matching, that the membrane and hemoglobin contributions occur at different length scales and although membrane scattering can not be eliminated stricto-sensus because of its inhomogeneity (the membrane contains lots of different protein) both signals can be easily separated. The dynamics of hemoglobin was studied inside red blood cells by neutron spin-echo spectroscopy [3] and more recently using time-of-flight spectrometry [76]. For contrast reasons, the first study was performed using red blood cells, which have been dialysed against D_2O, at the physiological temperature of 37°C from $Q \sim 0.02\text{Å}^{-1}$ to $Q \sim 0.13\ \text{Å}^{-1}$. This wave vector range

Author's Proof

surrounds the protein structure factor maximum, which means, that it ranges from typically intermolecular distances up to few tens of nanometers. The results can be summarised as follows [3]:

- The diffusion coefficient of hemoglobin in the red blood cells is equal to $D_s = 1.75(\pm 0.2).10^{-7}\text{cm}^2.\text{s}^{-1}$, in heavy water and at $T = 37°\text{C}$. When corrected for temperature and the viscosity difference between H_2O and D_2O, this leads to an equivalent of $D_s = 1.1(\pm 0.2).10^{-7}\text{cm}^2.\text{s}^{-1}$ in water at $T = 20°\text{C}$.
- The diffusion of hemoglobin at high concentration can be understood on the basis of theoretical concepts developed for colloidal suspensions. The main difference is that the effective hydrodynamic volume fraction of the protein must include the hydration shell because of the highest surface over volume ratio of the proteins.
- The protein–protein friction in the RBCs is mainly controlled by hydrodynamic interactions. This conclusion is based on the wave vector dependence of the apparent diffusion coefficient, and cannot be deduced only from the volume fraction dependance of $D_s(\Phi)$, because it can be reproduced by Brownian dynamics simulations of protein without hydrodynamic interactions.

The time-of-flight spectra were measured on D_2O-exchanged solutions (in order to reduce the contribution of the solvent) in the wave vector range $Q = 0.5\ \text{Å}^{-1}$ to $Q = 1.6\ \text{Å}^{-1}$ for different temperatures [76]. The analysis was similar to the one developed previously for protein solutions [77] in order to separate the contributions from Brownian diffusion and internal motions. The resolution of the spectrometer was set to a minimum of 41 µev and reaches more than 60 µev (Full-Width Half Maximum) at high angles. The line width of the Brownian diffusion contribution follows a characteristic Q^2 dependence at intermediate wave vectors but seems to saturate to a plateau around 4 µev for $Q^2 \leq 0.75\ \text{Å}^{-2}$. At high wave vectors, the authors claim that the curves show an inflection as is predicted theoretically for a jump diffusion models [78] (figure [76]).

The diffusion coefficient extracted from the Q^2 regime is similar to the one measured at infinite dilution D_o, by DLS and by macroscopic methods [56]. Perez et al. [77] estimated, in a different way to that described above, the contribution of rotational Brownian motions to the apparent diffusion coefficient in low concentration protein solutions measured by incoherent scattering. They used numerical integration of the Sears calculation for the contribution to the dynamical structure factor of the rotational diffusion of protons on a sphere [79, 80]. They concluded that rotational diffusion leads to an apparent increase of the translational diffusion coefficient and that $D_s \simeq D^{app}/1.27$. This calculation is valid for low protein concentration when the Stokes–Einstein laws occur for both translational and rotational Brownian diffusion, and reads for a sphere:

$$D_o = \frac{k_B T}{6\pi\eta R_H} \tag{8.26}$$

$$D_r = \frac{k_B T}{8\pi\eta R_H^3} \tag{8.27}$$

UNCORRECTED PROOF

Author's Proof

One should notice that the dimensions of both diffusion coefficients is not the same since $\langle r^2 \rangle = 6D_s t$, whereas $\langle \delta\theta^2 \rangle = 4D_r t$. Generally for diffusion in solution D_s is given in $cm^2.s^{-1}$ and D_r in s^{-1}.

The application to high concentration solutions is not straightforward because in general the Stokes–Einstein relations break down at high concentrations. For example in red blood cells the rotational diffusion coefficient is reduced by a factor of 2 [70], whereas the long-range translational one decreases by a factor of 7 [3]. The two type of motions do not experience the same influence of protein–protein interactions. In the chapter [76] the same procedure was applied to the short-time diffusion coefficient which is theoretically reduced ($D_s^s \simeq 0.56 D_o$) by as much as the rotational diffusion time, although it is closer to 0.34 when including the water hydration shell in the computation of the hydrodynamic volume.

The plateau at small wave vectors and the apparent saturation at high Q have been interpreted as a confinement due to the neighbouring molecules and a jump diffusion mechanism. The plateau at small wave vectors would mean that up to a certain distance the protein is freely diffusing with a coefficient D_s^S, then would be confined for a certain time, and after a time higher than the interaction time would diffuse over long range but with a decreased diffusion coefficient D_s^L. In terms of intermediate scattering function, I(Q,t), this would lead to a two time decay function with a plateau corresponding to the EISF of the protein's centre of mass. In fact, to get such a function the two characteristic times should be clearly time separated (more than one to two orders of magnitude), which is clearly not the case because the short- and long-time diffusion coefficients differ only by a factor from 2 to 3 at this concentration. Second, the full decay of I(Q,t) was measured by NSE [3] and did not show such a behaviour. The jump diffusion model assumes that the jumping time can be neglected with respect to the residence time; the authors calculate both times as $\tau_r \simeq 280$ ps for the residence time and $\tau_r \simeq 50$ ps. In fact, the picture is certainly closer to the traditional I(Q,t) for colloidal suspension at this volume fraction, a stretched decay function, the short time diffusion coefficient being obtained from the first cumulant analysis of the function, whereas the full decay occur with the long-time diffusion coefficient. Measuring such complicated decay functions is easier in the time domain, the convolution by the resolution function in the energy range could lead to erroneous conclusions.

8.3.4.5 Coupling of Internal and Diffusive Motions

Recently, a method was developed that allows to study the protein domain dynamics by an analysis of the departure from the DQ^2 law that is generally observed when only translational motions contribute to the signal [81, 82]. The method is not straightforward and involves sophisticated data treatments, since the effect of structure factor, hydrodynamic factor and rotational motions, must first be eliminated from the measured signal (i.e. the apparent diffusion coefficient $D_{\text{eff}}(Q)$), although the calculation is simplified by the low concentrations of protein in solution.

UNCORRECTED PROOF

Author's Proof

In [82], the authors studied the interdomain motion in Alcohol dehydrogenase (ADH). From the effective diffusion coefficient $D_{\text{eff}}(Q)$, a single tetramer effective diffusion coefficient is deduced using the classical Ackerson formula [39]: $D^{\text{o}}_{\text{eff}}(Q) = D_{\text{eff}}(Q) * S(Q)/H(Q)$. The prime reason for the Q modulation $D^{\text{o}}_{\text{eff}}(Q)$ is the rotational Brownian diffusion of the aspherical tetramer, which can be calculated using the computer code HYDROPRO [83]. Finally the difference between the calculated and the measured single effective diffusion coefficient $\Delta D^{\text{o}}_{\text{eff}}(Q)$ is compared with the non trivial lower frequency mode normal calculation and some motions prevailing can be identified (see figure do we insert a figure of prl 101 138102?).

8.3.5 Conclusion

Dynamics are fundamental for proteins to achieve their functions. Stochastic processes, driven by Brownian noise are of primary importance from a molecular level, acting as plasticizers, up to the cell where their unbalanced effects lead to transport and protein motions. These processes span from the picoseconds, as for example, water diffusion or small group internal motions, up to long time large domain fluctuations, associated to functions and protein diffusion. Neutron scattering is a valuable tool for the investigation of the dynamics of proteins and hence the correlation between these motions and protein function. Internal and global motions can be separated by appropriate sample choice (for example hydrated powder to study internal dynamics without translational diffusion) or spectrometer configurations. A general rule is to extend the energy (or time) range of investigation as far as possible by combining different types of spectrometer. Inelastic or quasielastic, neutron scattering can span over 7 or 8 orders of magnitude in time. A particular difficulty is to combine measurements in the time domain, as is the case with neutron spin-echo, with broader bandwidth measurements in the energy domain (Time-of-flight, backscattering). The transformation from energy ($\hbar\omega$) to the time domain is not straightforward and needs a careful account of the $\hbar\omega - Q$ windows of the spectrometer as well as their resolution shapes or even coherent to incoherent ratios. It is sometimes interesting if not necessary to refine models to spectra obtained with different spectrometer configurations or even different types of spectrometer. Using the refined parameters obtained at low resolution as input for the refinements of the high resolution and so on. Such procedure has the advantage of allowing the test of models over a wide range of wave vector and energy transfer. In any case, strategies must be developed to study a specific type of motion over the entire domain it spans and eventually to study the coupling with other motions.

UNCORRECTED PROOF

Author's Proof

References

1. B. Jacrot. Study of biological structures by neutron scattering from solution. *Rep. on Prog. in Physics*, 39:911–953, 1976.
2. W. Doster, S. Cusack, and W. Petry. Dynamical transition of myoglobin revealed by inelastic scattering. *Nature*, 337:754–756, 1989.
3. W. Doster and S. Longeville. Microscopic diffusion and hydrodynamic interactions of hemoglobin in red blood cells. *Biophys. J*, 93:1360–1368, 2007.
4. W. Doster and M. Settles. Protein-water displacement distributions. *Biochim. Biophys. Act.*, 1749:173–186, 2005.
5. H. Lichtengegger, W. Doster, T. Kleinert, A. Birk, B. Sepiol, and G. Vogl. Heme-solvent coupling, a mossbauer study of myoglobin in sucrose. *Biophys. J.*, 76:595–603, 1999.
6. R.F. Tilton, I. D. Kunz, and G.A. Petsko. Cavities in proteins. *Biochem.*, 23:2849–2857, 1984.
7. M. Brunori and Q. H. Gibson. Cavities and packing defects in the structural dynamics of myoglobin. *EMBO reports*, 2,8:674–679, 2001.
8. V. Srajer, T. Y. Teng, T. Ursby, C. Pradervand, Z. Ren, S. Adachi, W. Schildkamp, D. Bourgeois, M. Wulff, and K. Mofat. Photolysis of the carbon monoxide complex of myoglobin: nano-second time-resolved crystallography. *Science*, 274:1726–1729, 1996.
9. F. Schotte, M. Lim, T. A. Jackson, A. V. Smirnov, J. Soman, J. S. Olson, G. N. Phillips, M. Wullff, and P.A. Anfinrud. Watching a protein as it functions with 150 ps time-resolved X-ray crystallography. *Science*, 300:1944–1947, 2003.
10. A. Tomita, T. Sato, and S. Nozawa K. Ichiyanagi, H. Ichikawa, M. Chollet, F. Kawai, S.-Y. Park, T. Yamato T. Tsuduki, S. y. Koshihara, and S. i. Adachi. Visualizing breathing motion of internal cavities in concert with ligand migration in myoglobin. *Proc. Natl. Acad. Sci.*, 106:2612–2616, 2009.
11. R. Elber and M. Karplus. Enhanced sampling in molecular dynamics: use of the time dependent hartree approximation for a simulation of carbon monoxide diffusion through myoglobin. *J. Am. Chem. Soc.*, 112:9161–9175, 1990.
12. J. Cohen, A. Arkhipov, R. Braun, and K. Schulten. Imaging the migration pathway for o_2, co, no and ce inside myoglobin. *Biophys. J.*, 91:1844–1857, 2006.
13. Th. Kleinert, W. Doster, H. Leyser, W. Petry, V. Schwarz, and M. Settles. Solvent composition and viscosity effects on the kinetics of co-binding to horse myoglobin. *Nature*, 37:717–733, 1998.
14. W. Doster. The protein-solvent glass transition. *Bioch. Biophys. Act.*, 1804:3–14, 2010.
15. A. Ansari, C. Jones, E. R. Henry, J. Hofrichter, and M. A. Eaton. The role of solvent viscosity in the dynamics of protein conformational-changes. *Science*, 256:1796–1796, 1992.
16. D. Beece, L. Eisenstein, H. Frauenfelder, D. Good, M. Marden, L. Reinisch, A. Reynolds, L. Sorenson, and K. Yu. Viscosity and protein dynamics. *Biochem.*, 19:5147–5157, 1980.
17. S. N. Timasheff. Protein hydration, thermodynamic binding and preferential hydration. *Biochem.*, 41:13473–13482, 2002.
18. F. Parak and E.W. Knapp. A consistent picture of protein dynamics. *Proc. Natl. Acad. Sci. USA*, 81:7088–7092, 1984.
19. F. Parak and K. Achterhold. Protein dynamics on different timescales. *J. of Phys. and Chem. of Solids*, 66:2257–2262, 2005.
20. W. Doster. *Brownian oscillator analysis of molecular motions in biomolecules, in Neutron Scattering in Biology*. Ed. J. Fitter, T. Gutberlet and J. Katsaras, Springer Series Biological and Medical Physics, Biomedical Engeneering., 2005.
21. W. Doster. Dynamic structural distibutions in proteins. *Physica B*, 385-386:831–834, 2006.
22. R. H. Roh, V. N. Novikov, R. B. Gregory, J. E. Curtis, Z. Chaowduri, and A. P. Sokolov. Onset of harmonicity of protein dynamics. *Phys. Rev. Lett.*, 95:038101–038103, 2005.
23. J. Zaccai. How soft is a protein? a protein force constant measured by neutron scattering. *Science*, 288:1604–1607, 2000.

AQ9

UNCORRECTED PROOF

Author's Proof

24. W. Doster. *Dynamical transition of proteins, the role of hydrogen bonds: in Hydration Processes in Biology*. (Les Houches Lectures) Ed. Marie-Claire Bellissent-Funel, IOS Press., 1998.
25. W. Doster. The dynamical transition of proteins, concepts and misconceptions. *Eur. Biophys. J.*, 37:591–602, 2008.
26. W. Doster, M. Diehl, W. Petry, and M. Ferrand. Elastic resolution spectroscopy: a method to study molecular motions in small biological samples. *Physica B*, 301:65–68, 2001.
27. W. Doster, M. Diehl, R. Gebhardt, R.E. Lechner, and J. Pieper. Elastic resolution spectroscopy: a method to study molecular motions in small biological samples. *Chem. Phys.*, 292:487–494, 2003.
28. M. Settles and W. Doster. Anomalous diffusion of protein hydration water. *Faraday Discussions*, 103:269–279, 1996.
29. A. Paciaroni, S. Cinelli, and G. Onori. Effect of the environment on the protein dynamical transition, a neutron scattering study. *Biophys. J.*, 83:1157–1164, 2002.
30. G. Onori E. Cornicchi and A. Paciaroni. Picosecond time scale fluctuations of proteins in glassy matrices: the role of viscosity. *Phys. Rev. Lett.*, 95:158104, 2005.
31. W. Doster, S. Busch, M.S. Appavou, A. Gaspar, J. Wuttke, and J. Scheer. The dynamical transition of protein hydration water. *Phys. Rev. Lett.*, Accepted, 2010.
32. R. H. Austin, K. W. Beeson, L. Eisenstein, H. Frauenfelder, and I. C. Gunsalus. Dynamics of ligand binding to myoglobin. *Biochem.*, 14:5355–5373, 1975.
33. F. Post, W. Doster, G. Karvounis, and M. Settles. Structural relaxation and nonexponential kinetics of ligand binding to horse myoglobin. *Biophys. J.*, 64:1833–1844, 1993.
34. D.A. Neumann A.M. Tsai and L.N. Bell. Molecular dynamics of solid state lysozyme as affected by glycerol and water: a neutron scattering study. *Biophys. J.*, 79:2728–2732, 2000.
35. F. Demmel, W. Doster, W. Petry, and A. Schulte. Vibrational frequencies as a probe of hydrogen bonds: thermal expansion and glass transition of myoglobin in mixed solvents. *Eur. Biophys. J.*, 26:327–335, 1997.
36. G. D. J. Phillies. Effects of intermolecular interactions on diffusion .1. 2-component solutions. *J. Chem. Phys.*, 60:976–982, 1974.
37. G. D. J. Phillies. Continuum hydrodynamic interactions and diffusion. *J. Chem. Phys.*, 62:3925–3932, 1975.
38. P. N. Pusey. Scaled particle theory of fluid mixtures. *J. Phys. A: Math. Nucl. Gen.*, 8: 1433–1440, 1975.
39. B. J. Ackerson. Correlations for interacting brownian particles. *J. Chem. Phys.*, 64:242–246, 1976.
40. B. J. Ackerson. Correlations for interacting brownian particles. 2. *J. Chem. Phys.*, 69:684–690, 1978.
41. C. W. J. Beenakker and P. Mazur. Self-diffusion of spheres in a concentrated suspension. *Physica*, 120A:388–410, 1983.
42. C. W. J. Beenakker and P. Mazur. Diffusion of spheres in a concentrated suspension 2. *Physica*, 126:349–370, 1984.
43. M. Médina-Noyola. Long-time self-diffusion in concentrated colloidal dispersions. *Phys. Rev. Lett*, 60:2705–2708, 1988.
44. M. Tokuyama and I. Oppenheim. Dynamics of hard sphere suspension. *Phys. Rev. E*, 50: R16–R19, 1994.
45. J. B. Hayter and J. Penfold. An analytical struture factor for macroion solutions. *Mol. Physics*, 42:109–118, 1981.
46. J. P. Hansen and J. B. Hayter. A rescaled msa structure factor for dilute charged collodal dispersions. *Molecular Physics*, 46:651–656, 1982.
47. L. Belloni. Electrostatic interactions in collodal solutions - comparaison between primitive and one-component model. *J. Chem. Phys.*, 85:519–526, 1986.
48. J. A. Dix and A. S. Verkman. Crowding effects on diffusion in solutions and cells. *Annu. Rev. Biophys.*, 37:247–263, 2008.

AQ10

UNCORRECTED PROOF

Author's Proof

49. M. Carmo-Fonseca, M. Platani, and J. R. Sweldow. Macromolecular mobility inside cell nucleus. *TRENDS in Cell Biology*, 12:491–495, 2002.
50. J. Lippincott-Schwartz, E. Snapp, and A. Kenworthy. Studying protein dynamics in living cells. *Nature*, 2:444–456, 2001.
51. R. D. Phair and T. Misteli. High mobility of proteins in the mamalian cell nucleus. *Nature*, 404:604–609, 2000.
52. D. Bendedouch and S.-H. Chen. Structure and interparticle interactions of boviner serum albumin in solution studied by small-angle neutron scattering. *J. Phys. Chem.*, 87:1473–1477, 1983.
53. S. Krueger and R. Nossal. Sans studies of interacting hemoglobin in intact erythrocytes. *Biophys. J*, 53:97–105, 1988.
54. S. Krueger, S.-H. Chen, J. Hofrichter, and R. Nossal. Small-angle neutron-scattering studies of hba in concentrated solutions. *Biophys. J*, 58:745–757, 1990.
55. S. Longeville, W. Doster, and G. Kali. Myoglobin in crowded solutions: structure and diffusion. *Chem. Phys.*, 292:413–424, 2003.
56. V. Riveros-Moreno and J. B. Wittenberg. Self-diffusion coefficients of myoglobin and hemoglobin in concentrated solutions. *The J. of Biological Chemistry*, 247:895–901, 1972.
57. S. S. Alpert and G. Banks. The concentration dependence of the hemoglobin mutual diffusion coefficient. *Biophys. Chem.*, 4:287–296, 1976.
58. R. S. Hall and C. S. Johnson. Experimental-evidence that mutual and tracer diffusion-coefficients for hemoglobin are not equal. *J. Chem. Phys.*, 72:4251–4253, 1980.
59. S. Longeville, W. Doster, M. Diehl, R. Gaehler, and W. Petry. Neutron resonance spin echo : Oxygen transport in crowded protein solutions. *in Neutron Spin Echo Spectroscopy, Basic trends and Applications*, Lecture Notes in Physics, vol 601 Eds F. Mezei, C. Pappas and T. Gutberlet, Springer, Berlin, 2003:325–335, 2003.
60. C. Le Coeur, B. Demé, and S. Longeville. The compression of random coils due to macro-molecular crowding. *Phys. Rev. E*, 79:031910, 2009.
61. W. Haeussler. Structure and dynamics in apoferritin solutions with paracrystalline order. *Chem. Phys.*, 292:425–434, 2003.
62. W. Haeussler and B. Farago. Diffusive dynamics in ordered solutions of apoferritin solutions near the structure factor peaks. *J. Phys.: Condens. Matter*, 15:S197–S204, 2003.
63. A. J. Banchio, J. Gapinsky, A. Patkowski, W. Haeussler, A. Fluerasu, S. Sacanna, P. Holmqvist, G. Meier, M. P. Lettinga, and G. Naegele. Many-body hydrodynamic interactions in charged-stabilized suspensions. *Phys. Rev. Lett.*, 96:138303, 2006.
64. W. Haeussler. Neutron spin echo studies on ferritin: free-particle diffusion and interacting solutions. *Eur. Biophys. J.*, 37:563–571, 2008.

AQ11 65. J. Gapinski, A. Wilk, A. Patkowski, W. Haussler, A. J. Banchio, R. Pecora, and G. N/.

66. N. Muramatsu and A. P. Minton. Tracer diffusion of globular-proteins in concentrated protein solutions. *Proc. Natl. Acad. Sci. USA*, 85:2984–2988, 1988.
67. P. D. Ross and A. P. Minton. Hard quasispherical model for the viscosity of hemoglobin solutions. *Biochemical and biophysical reasearch communications*, 76:971–976, 1977.
68. W. van Megen, S. M. Underwood, and I. Snook. Tracer diffusion in concentrated colloidal suspension. *J. Chem. Phys.*, 85:4065–4072, 1986.
69. P. N. Pusey. *Colloidal suspensions, in Liquids, Freezing and Glass transition*. J.P. Hansen, D. Levesque and J. Zinn-Justin, eds, North Holland Pub., 1991.
70. D. Lavalette, C. Tetreau, M. Tourbez, and Y. Blouquit. Microscopic viscosity and rotational diffusion of proteins in a macromolecular environment. *Biophys. J.*, 76:2744–2751, 1999.
71. C. Le Coeur and S. Longeville. Microscopic protein diffusion at high concentration by neutron spi-echo spectroscopy. *Chem. Physics*, 345:298–304, 2008.
72. P.-G. de Gennes. Liquid dynamics and inelastic scattering of neutrons. *Physica*, 25:825, 1959.
73. C. R. Jones, C. S. Johnson, and Penniston J. T. Photon correlation spectroscopy of hemoglobin - diffusion of oxy-hba and oxy-hbs. *Biopolymers*, 17:1581–1593, 1978.

UNCORRECTED PROOF

Author's Proof

74. C. H. Everheart and C. S. Johnson. Pulse field gradient nmr determination of the temperature dependence of the tracer diffusion coefficient of hemoglobin. *Biopolymers*, 21:2049–2054, 1982.
75. P. W. Kuchel and B. E. Chapman. Translational diffusion of hemoglobin in human erythrocytes and hemolysates. *Journal of magnetic resonance*, 94:574–580, 1991.
76. A. M. Stadler, I. Digel, G. M. Artmann, J. P. Embs, G. Zaccai, and G. Bueldt. Hemoglobin dynamics in red blood cells: correlation to body temperature. *Biophysical J.*, 95:5449–5461, 2008.
77. J. Perez, J.-M. Zanotti, and D. Durand. Evolution of the internal dynamics of two globular proteins from dry powder to solution. *Biophys. J.*, 77:454–469, 1999.
78. K. S. Singwi and A. Sjoelander. Resonance absorption of nuclear gamma rays and the dynamics of atomic motions. *Phys. Rev.*, 120:1093–1102, 1960.
79. V. F. Sears. Cold neutron scattering by homonuclear diatomic liquid: 1 free rotation. *Can. J. Phys.*, 44:1279, 1966.
80. V. F. Sears. Cold neutron scattering by homonuclear diatomic liquid: 2 hindred rotation. *Can. J. Phys.*, 44:1999, 1966.
81. Z. Bu, R. Biehl, M. Monkenbusch, D. Richter, and D. J. E. Callaway. Coupled protein domain motion in taq polymerase revealed by neutron spin-echo spectroscopy. *Proc. Nat. Acad. Sci.*, 102:17646–17651, 2005.
82. R. Biehl, B. Hoffmann, M. Monkenbusch, P. Falus, S. Préost, R. Merkel, and D. Richter. Direct observation of correlated interdomain motion in alcohol dehydrogenase. *Phys. Rev. Lett.*, 101:138102, 2008.
83. M. L. Huertas J. G. de la Torre and B. Carrasco. Calculation of hydrodynamic properties of globular proteins from their atomic-level structure. *Biophys. J.*, 78:719–730, 2000.

UNCORRECTED PROOF

Author's Proof

AUTHOR QUERIES

AQ1. First author has been considered as the corresponding author.
AQ2. Please check if the insertion of ", etc." in the sentence "To is separate ….." is appropriate.
AQ3. Please confirm if you need l figure in colour.
AQ4. Please provide missing for open bracket.
AQ5. Please provide citation in the sentence "It is ofte claimed …"
AQ6. Citation is missing after "Green Fluorescence protein", Please check.
AQ7. Short-time diffusion is given in lower case and upper case. Please check. Also, please note that in the sentence "Under these conditions…" it is represented before 'D' elsewhere it is given after 'D'.
AQ8. Please provide citation in the sentence "P. Segré and P. Pusey.…"
AQ9. Please update ref. 20.
AQ10. Please update ref. 31.
AQ11. Please provide complete details for ref. 65.

UNCORRECTED PROOF